The Origin and Evolution of Saturn, with Exoplanet Perspective
By Sushil K. Atreya, Aurélien Crida, Tristan Guillot, Jonathan I. Lunine, Nikku Madhusudhan, Olivier Mousis (2019). pp 5-43, in *Saturn in the 21st Century* (eds. KH Baines, FM Flasar, N Krupp, T Stallard), Cambridge University Press. https://doi.org/10.1017/9781316227220.002.

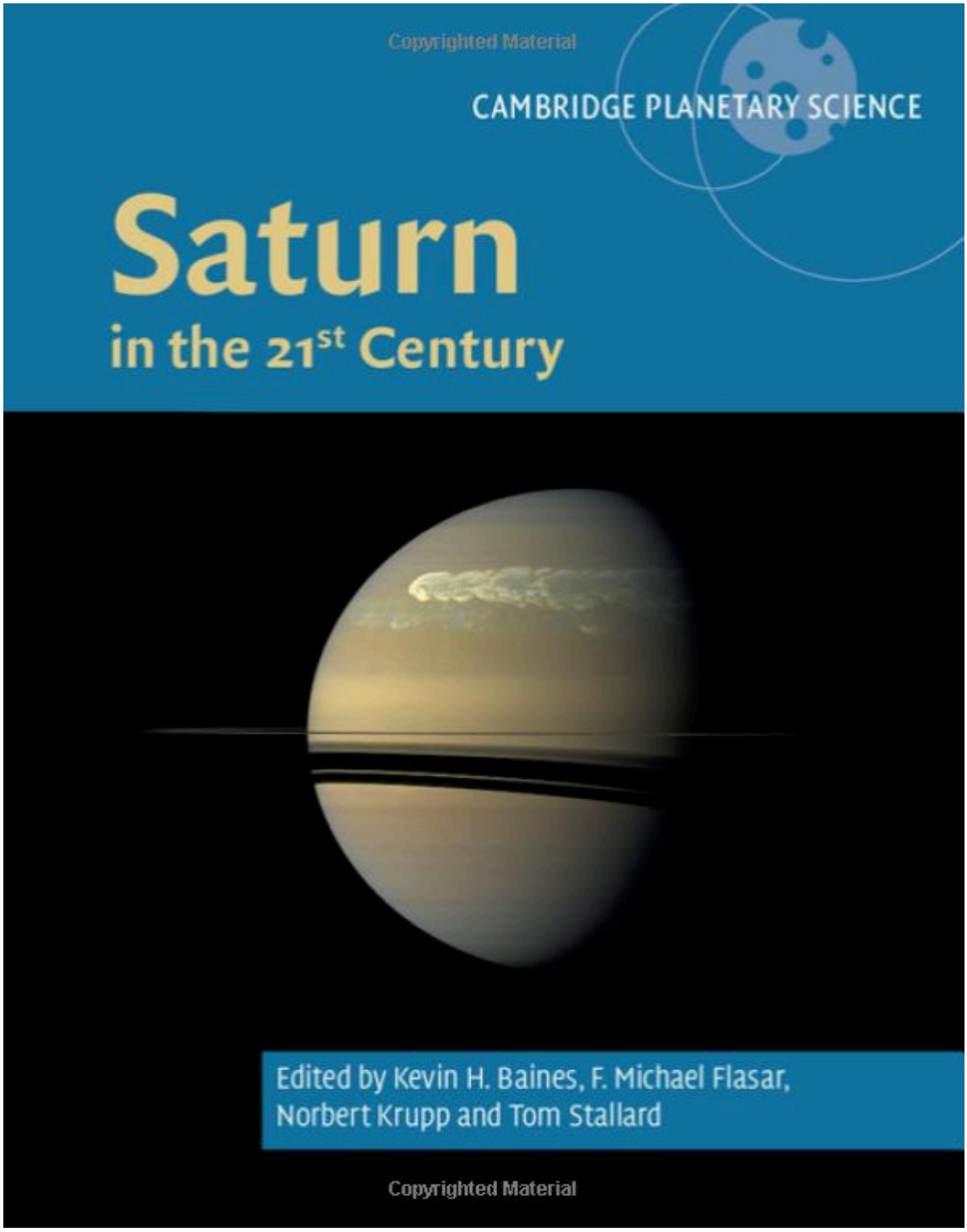

2

The Origin and Evolution of Saturn, with Exoplanet Perspective

SUSHIL K. ATREYA, AURÉLIEN CRIDA, TRISTAN GUILLOT, JONATHAN I. LUNINE, NIKKU MADHUSUDHAN AND OLIVIER MOUSIS

Abstract

Saturn formed beyond the snow line in the primordial solar nebula, and that made it possible for it to accrete a large mass. Disk instability and core accretion models have been proposed for Saturn's formation, but core accretion is favored on the basis of its volatile abundances, internal structure, hydrodynamic models, chemical characteristics of protoplanetary disk, etc. The observed frequency, properties, and models of exoplanets provide additional supporting evidence for core accretion. The heavy elements with mass greater than ^{4}He make up the core of Saturn, but are presently poorly constrained, except for carbon. The C/H ratio is super-solar, and twice that in Jupiter. The enrichment of carbon and other heavy elements in Saturn and Jupiter requires special delivery mechanisms for volatiles to these planets. In this chapter we will review our current understanding of the origin and evolution of Saturn and its atmosphere, using a multifaceted approach that combines diverse sets of observations on volatile composition and abundances, relevant properties of the moons and rings, comparison with the other gas giant planet, Jupiter, and analogies to the extrasolar giant planets, as well as pertinent theoretical models.

2.1 Introduction

Saturn, though about one-third the mass of Jupiter, is the largest planetary system in the solar system, considering the vast reach of its rings and dozens of known moons. Thus, Saturn is key to understanding the origin and evolution of the solar system itself. Models, observations, comparison with Jupiter, the other gas giant planet, and analogies with extrasolar giant planets have begun to give a sense of how Saturn, in particular, and the giant planets in general, originated and evolved.

Two distinct mechanisms of giant planet formation have been proposed in the literature: (1) disk instability and (2) nucleated instability (or core accretion). The latter goes back to papers by Hayashi (1981) and his colleagues (e.g. Mizuno 1980), and requires the accretion of a solid body (rock/metal, ice, and, possibly, refractory organics) up to a critical mass threshold at which rapid accretion of gas becomes inevitable – typically 10 times the mass of the Earth (see Armitage 2010, for a discussion). The former theory had its origin in the 1970s (see Cameron 1979) for hot, massive disks, but it was determined later (Boss 2000; Mayer et al. 2002) that the instabilities required to break up a portion of a gaseous disk into clumps are a feature of cold, massive disks. We will focus on each of these contrasting models in turn, and then discuss the observational indicators in our own and extrasolar planetary systems that might distinguish between the two models.

The disk instability model is based on numerical simulations showing that massive, relatively cold disks will spontaneously fragment due to a gravitational instability, leading to multiple discrete, self-gravitating masses. In computer simulations of the process these features seem somewhat ill defined, and it is not possible to track the subsequent condensation of these features in the same hydrodynamical simulation that tracks the onset of the instability itself.

Nonetheless, basic disk physics dictates that such fragmentation will occur for a sufficiently massive or cold disk (Armitage 2010) and that the timescale for the fragmentation, once the instability does occur, is extremely short – hundreds to thousands of years.

Once formed, the fragments (assuming they continue to contract to form giant planets) are usually sufficiently numerous that the aggregate planetary system is dynamically unstable. The planets will gravitationally interact, scattering some out of the system and leaving the others in a variety of possible orbits. The evidence from microlensing of a substantial population of free-floating Jupiter-mass objects (Sumi et al. 2011) not associated with a parent star constitutes one argument in favor of the importance of this formation mechanism.

On the other hand, it is not evident how giant planets formed by the disk instability mechanism acquire significant amounts of heavy elements over and above their parent star's abundances. It has been argued that subsequent accretion of planetesimals would generate the increased metallicity, but the disruption of the disk associated with the gravitational instability might have removed the raw material for large amounts of planetesimals – the materials going into numerous giant planets that are then kicked out of the system. A subsequent phase of disk building or direct accretion of planetesimals from the surrounding molecular cloud may have to be invoked. And this begs the question of core formation – giant planets formed in this way may have super-solar metallicities but lack a heavy element core unless (as seems unlikely) very large (Earth-sized) planets are consumed by these objects.

The core accretion model, in contrast, begins by building a heavy element core through planetesimal and embryo accretion in the gaseous disk (embryo is usually reserved for lunar-sized bodies and upward). At some point, the gravitational attraction of the large core leads to an enhanced accretion of gas, so much so that gas accretion quickly dominates in a runaway process and the object gains largely nebular-composition gas until its mass is large enough to create a gap in the disk and slow accretion. Such a model produces, by definition, a heavy element core, and through co-accretion of gas and planetesimals, an envelope enrichment of heavy elements as well. The model's Achilles heel is the time required to build the heavy element core to the point where rapid gas accretion occurs – millions of years or more. The onset of rapid gaseous accretion, by which point further growth may be rapid, depends not only on the core accretion rate but also, through the critical core mass (roughly 10 M_E, where M_E is an Earth mass) needed to trigger rapid gas accretion, the envelope opacity, and hence metallicity. Furthermore, the core accretion rate itself is a sensitive function of what one assumes about the planetesimal size distribution and surface density in the disk.

A plausible timescale for the formation of Saturn must be consistent with the lifetime of gas in disks, but may also be constrained by the 3–5 million-year (Myr) estimate of the formation duration of Iapetus, from its geophysical shape and thermal history (Castillo-Rogez et al. 2009). Earliest models had lengthy formation times (e.g. 8 Myr; Pollack et al. 1996), but more recent models can make Saturn in a few million years by appropriate selection of nebular parameters such as grain distribution and opacity (Dodson-Robinson et al. 2008).

The overall history of the solar system and presence of a substantial terrestrial planet system inward of Jupiter and Saturn suggests that the extreme dynamical scattering suffered after disk instability protoplanets are formed did not happen in our solar system. Furthermore, if the 3–5-million-year estimate of the interval between the formation of the first solids and the formation of Iapetus (Castillo-Rogez et al. 2009) is correct, the disk instability – if it occurred – would have produced Saturn much too soon after (or even before) the first solids in the solar system condensed out. There is sufficient evidence that the first solids, millimeter-sized chondrules and calcium aluminum inclusions (CAIs) in chondrites, date back to 4.5682 Gyr (billion years) (Amelin et al. 2010), which provides clear evidence that submicron-sized interstellar grains were sticking and accumulating to form solids at the very beginning of the solar system.

Measurement by the Juno mission of the water abundance below the meteorology layer in Jupiter, tied to the abundances of other major elements measured by the Galileo probe, will also provide an indication of how much planetesimal material was accreted (Helled and Lunine 2014), and to some extent, the nature of the carrier species (e.g. Mousis 2012). Although it is possible to enrich the envelopes of the giant planets even in

the disk instability model by adding planetesimals much later, the presence of both a substantial (10 M_E) core and envelope enrichment of heavy elements would strongly militate in favor of the core accretion model. Saturn's core mass may be measured by Cassini, but an inventory of the envelope enrichment of heavy elements and measurement of the deep water abundance will have to await a future Saturn probe.

The core accretion model gets a boost also from observational surveys of exoplanets. An analysis of the frequency of planets with different masses, sizes, orbits, and host characteristics reveals that a greater percentage of giant planets are found around higher-metallicity stars, and smaller planets between Earth's and Neptune's mass far exceed Jupiter-sized planets (Howard 2013; Johnson et al. 2010). This is what one would expect if core accretion were prerequisite for planetary formation. Thus, for our planetary system, at least, core accretion seems to make more sense. Trying to constrain detailed formation mechanisms by matching orbital properties is much more difficult because of the profound effects of migration (Mordasini, et al. 2009; Ida et al. 2013 and references therein).

In addition to their occurrence rates and orbital characteristics, the masses, radii, and atmospheric volatile gas compositions of giant exoplanets may also provide important clues regarding their formation processes, and in turn, formation of Saturn and Jupiter in the solar system. With rapid advances in spectroscopic observations of exoplanets, a number of gases relevant to formation models, including water vapor, methane and carbon monoxide have been detected in several giant exoplanets (Section 2.5), revealing diversity in chemical abundances. For example, there are some planets (e.g. HD 209458b) with seemingly lower H_2O abundances than expected from solar elemental composition (e.g. Deming et al. 2013; Madhusudhan et al. 2011a, 2014a), while others (e.g. WASP-43b) appear consistent with super-solar H_2O (e.g. Kreidberg et al. 2014). The latter is consistent with super-solar abundance of measured heavy elements in Saturn and Jupiter (Section 2.2.1), with a good likelihood that their original cores were rich in water ice. On the other hand, WASP-12b – which indicates a C/O ratio (≥1) twice solar (~0.5) – argues for a core made up of largely carbon-bearing constituents. If this result is confirmed for a multitude of similar exoplanets, it would have important implications for their formation and the formation of the gas giant planets of the solar system. More generally, new theoretical studies are suggesting that the observable O/H, C/H, and, hence, C/O ratios in giant exoplanetary atmospheres can place powerful constraints on their formation and migration mechanisms, as discussed in Section 2.5.3.

2.2 Observational Constraints

The models of Saturn's formation and evolution are constrained by data presently available on the planet's chemical composition and its interior. This section elaborates on each of these aspects and forms the basis for the discussions in subsequent sections.

2.2.1 Elemental Composition of Saturn's Atmosphere and Comparison to Jupiter

The composition of Saturn's atmosphere has been measured by remote sensing from ground-based and Earth-orbiting telescopes and flyby and orbiting spacecraft for over half a century. These observations have been instrumental in revealing the chemical makeup of Saturn's stratosphere and upper troposphere. As a result, mole fractions of helium (He), methane (CH_4), and a number of its photochemical products including methyl radical (CH_3), ethane (C_2H_6), acetylene (C_2H_2), methyl acetylene (C_3H_4), and benzene (C_6H_6), ammonia (NH_3), hydrogen sulfide (H_2S), and those species that are in thermochemical disequilibrium in Saturn's upper troposphere and stratosphere such as phosphine (PH_3), carbon monoxide (CO), germane (GeH_4), and Arsine (AsH_3) have been measured to varying degrees of precision. Some of the most precise data have come from observations made by the Cassini spacecraft (Fletcher et al., this book) that attained orbit around Saturn in 2004 and will embark on proximal orbits toward the end of the mission in 2017 (Baines et al., this book).

The abundances of certain heavy elements (m/z $>^4$He) and their isotopes can be derived from their principal chemical reservoirs in the atmosphere. As discussed earlier, heavy elements are key to constraining the models of the formation of Saturn and its atmosphere. Current best data on the abundances of elements relative to hydrogen in Saturn are listed in

Table 2.1. As Jupiter, the other gas giant planet in the solar system, is a good analog for Saturn, we list for comparison also the elemental abundances in Jupiter's atmosphere.

Many more heavy elements have been determined at Jupiter, in contrast to Saturn, because of in situ Galileo Jupiter entry probe measurements from 1995. Enrichment factors of the elements relative to proto-solar values are also listed in Table 2.1, using currently available solar elemental abundances from two different sources (Asplund et al. 2009; Lodders et al. 2009). Further insight into key elemental abundances is given below, and the reader is referred also to the table footnotes.

After hydrogen, helium is the most abundant element in the universe, the sun, and the giant planets. Conventional thinking has been that the current abundance of helium ratioed to hydrogen in the giant planets should be the same as in the primordial solar nebula from which these planets formed, and originally the Big Bang, in which helium was created. Thus, precise determination of the helium abundance is essential to understanding the formation of the giant planets, in particular, and to shedding light on the solar nebula and the universe in general. Whereas helium has been measured very accurately at Jupiter by two independent techniques on the Galileo probe (Table 2.1), such is not the case for Saturn. In the absence of an entry probe at Saturn, helium abundance at Saturn was derived from atmospheric mean molecular weight (μ), using a combination of the Voyager infrared spectrometer (IRIS) and the radio science (RSS) investigations. RSS measured radio refractivity that provides the information on T/μ, where T is the temperature measured by both instruments.

Initial analysis using the IRIS-RSS data (Conrath et al. 1984) yielded a greatly sub-solar He/H=0.017 ±0.012 (He/H_2=2×He/H). Subsequent reanalysis of the data employing IRIS alone gave He/H between 0.055 and 0.08 (Conrath and Gautier 2000). The authors emphasize, however, the retrieval of He/H is non-unique, but strongly suggests a value significantly greater than the earlier result that was based on the combined IRIS-RSS approach. For the purpose of this chapter, we take an average of the range of Saturn's He/H of 0.055–0.08, and express it as 0.0675±0.0125 (Table 2.1), but with the caveat that the value could well change following detailed analysis of the Cassini CIRS data and, especially, future in situ measurements at Saturn, as did Jupiter's He/H_2 following in situ measurements by the Galileo probe compared to the value derived from Voyager's remote sensing observations. The current estimate of He/H in Saturn's upper troposphere is about 0.7× solar compared to Jupiter's 0.8× solar. The sub-solar He/H_2 in the tropospheres of Jupiter and Saturn presumably results from the removal of some fraction of helium vapor through condensation as liquid at 1–2 megabar pressure in the interiors of these planets, followed by separation of helium droplets from metallic hydrogen. The severe depletion of Ne observed by the Galileo probe (Table 2.1) in Jupiter is excellent evidence of the helium-hydrogen immiscibility layer, as helium droplets absorb neon vapor, separate from hydrogen, rain toward the core, and this results in the depletion of helium and neon in the upper troposphere (Roulston and Stevenson 1995; Wilson and Militzer 2010). Models predict that the cooler interior of Saturn is expected to result in a greater degree of helium condensation and therefore a tropospheric He/H_2 ratio lower for Saturn than for Jupiter. Although the central value for Saturn is smaller than Jupiter's, the large uncertainty of Saturn's result does not provide a definite answer. Helium differentiation in Saturn's interior is invoked also as a way to explain the planet's large energy balance (Conrath et al. 1989). Without such chemical differentiation, models predict the heat flux excess at Saturn to be about three times lower than observed (Grossman et al. 1980), but the equation of state for the high-pressure, high-temperature interior is uncertain, so the modeled excess is not that well constrained (see Chapter 3 by Fortney et al. for additional details). Saturn and Jupiter both emit nearly twice the thermal radiation compared to the radiation the absorb from the sun. Whereas the release of heat of accretion from conversion of the gravitational potential energy as these planets cool and contract over time accounts for a good fraction of the energy balance of Jupiter, helium differentiation may play a significant role at Saturn. Since helium is denser than hydrogen, gravitational potential energy available for conversion to heat increases as helium raindrops begin to separate from hydrogen and precipitate upon reaching centimeter size. In summary, there are indications that helium is depleted relative to solar in Saturn's

Table 2.1 *Elemental Abundances in Jupiter and Saturn and Ratios to Protosolar Values*

Elements	Jupiter	Saturn	Sun-Protosolar (Asplund et al. 2009) [a,b]	Jupiter/ Protosolar (using Asplund et al. 2009) [a,b]	Saturn/Protosolar (using Asplund et al. 2009) [a,b]	Sun-Protosolar (Lodders et al. 2009) [m]	Jupiter/ Protosolar (using Lodders et al. 2009) [m]	Saturn/ Protosolar (using Lodders et al. 2009) [m]
He/H	$7.85 \pm 0.16 \times 10^{-2}$ [c]	$5.5–8.0 \times 10^{-2}$ [i], taken as $6.75 \pm 1.25 \times 10^{-2}$	9.55×10^{-2}	0.82 ± 0.02	0.71 ± 0.13 (?)	9.68×10^{-2}	0.81 ± 0.02	0.70 ± 0.13 (?)
Ne/H	$1.24 \pm 0.014 \times 10^{-5}$ [d]		9.33×10^{-5}	0.13 ± 0.001		1.27×10^{-4}	0.098 ± 0.001	
Ar/H	$9.10 \pm 1.80 \times 10^{-6}$ [d]		2.75×10^{-6}	3.31 ± 0.66		3.57×10^{-6}	2.55 ± 0.50	
Kr/H	$4.65 \pm 0.85 \times 10^{-9}$ [d]		1.95×10^{-9}	2.38 ± 0.44		2.15×10^{-9}	2.16 ± 0.39	
Xe/H	$4.45 \pm 0.85 \times 10^{-10}$ [d]		1.91×10^{-10}	2.34 ± 0.45		2.1×10^{-10}	2.11 ± 0.40	
C/H	$1.19 \pm 0.29 \times 10^{-3}$ [e]	$2.65 \pm 0.10 \times 10^{-3}$ [j]	2.95×10^{-4}	4.02 ± 0.98	8.98 ± 0.34	2.77×10^{-4}	4.29 ± 1.05	9.56 ± 0.36
N/H	$3.32 \pm 1.27 \times 10^{-4}$ [e]	$0.80–2.85 \times 10^{-4}$ [k];	7.41×10^{-5}	4.48 ± 1.71 [e]	1.08–3.84;	8.19×10^{-5}	4.06 ± 1.55 [e]	0.98–3.48;
	$4.00 \pm 0.50 \times 10^{-4}$ [f]	$2.27 \pm 0.57 \times 10^{-4}$ with		5.40 ± 0.68 [f]	3.06 ± 0.77 with		4.89 ± 0.62 [f]	2.78 ± 0.73 with
	$2.03 \pm 0.46 \times 10^{-4}$ [g]	$fNH_3=4 \pm 1 \times 10^{-4}$		2.70 ± 0.60 [g]	$fNH_3=4 \pm 1 \times 10^{-4}$		2.50 ± 0.55 [g]	$fNH_3=4 \pm 1 \times 10^{-4}$
O/H	$2.45 \pm 0.80 \times 10^{-4}$ [e]		5.37×10^{-4}	0.46 ± 0.15 (hotspot)		6.07×10^{-4}	0.40 ± 0.13 (hotspot)	
S/H	$4.45 \pm 1.05 \times 10^{-5}$ [e]	1.88×10^{-4} [l]	1.45×10^{-5}	3.08 ± 0.73	13.01	1.56×10^{-5}	2.85 ± 0.67	12.05
P/H	$1.08 \pm 0.06 \times 10^{-6}$ [h]	$3.64 \pm 0.24 \times 10^{-6}$ [h]	2.82×10^{-7}	3.83 ± 0.21	12.91 ± 0.85	3.26×10^{-7}	3.30 ± 0.18	11.17 ± 0.74

[a] Protosolar values calculated from the solar photospheric values of Asplund et al. (2009, table 1).

[b] According to Asplund et al. (2009), the protosolar metal abundances relative to hydrogen can be obtained from the present-day photospheric values (table 1 of Asplund et al. 2009) increased by +0.04 dex, i.e. ~11%, with an uncertainty of ±0.01 dex; the effect of diffusion on He is very slightly larger: +0.05 dex (±0.01). Note that Grevesse et al. (2005, 2007) used the same correction of +0.05 dex for all elements (dex stands for "decimal exponent," so that 1 dex=10).

[c] von Zahn et al. (1998), using helium detector on Galileo Probe; independently confirmed by the Galileo Probe Mass Spectrometer (GPMS, Niemann et al. 1998).

[d] Mahaffy et al. (2000); Kr and Xe represent the sum of all isotopes except for ^{126}Xe and ^{124}Xe that could not be measured by the GPMS but are probably negligible, as together they make up 0.2% of the total xenon in the sun.

(e) Wong et al. (2004), based on re-calibration of the GPMS data on CH_4, NH_3, H_2O, and H_2S down to 21 bars, using an experiment unit; represents an update of the values reported in Niemann et al. (1998) and Atreya et al. (1999, 2003).

(f) Folkner et al. (1998), by analyzing the attenuation of the Galileo probe-to-orbiter radio communication signal (L-band at 1387 MHz or 21.6 cm) by ammonia in Jupiter's atmosphere.

(g) Juno microwave radiometer (MWR) preliminary result in the equatorial region and two different longitudes (Bolton et al. 2017).

(h) Fletcher et al. (2009a) derived global PH_3 mole fractions of 1.86±0.1 ppm and 6.41±0.42 ppm, respectively, in the upper tropospheres of Jupiter and Saturn from an analysis of the mid-IR emission measured by the Cassini Composite Infrared Spectrometer (CIRS).

(i) Conrath and Gautier (2000) give a range of 0.11–0.16 for the He/H_2 mole fraction from re-analysis of the Voyager IRIS data at Saturn, but the result is tentative. We use an average He/H=0.0675 for the purpose of calculating the ratios of other elements relative to hydrogen in Saturn.

(j) Fletcher et al. (2009b) report mole fraction of $CH_4=4.7\pm0.2\times10^{-3}$ from an analysis of the CIRS data.

(k) Fletcher et al. (2011), using VIMS data giving an ammonia mole fraction, $f NH_3$, in the 1–3 bar region that is 140±50 ppm (scattering), 200±80 ppm (non-scattering) and rises to 300–500 ppm at the equator. If the maximum in ammonia measured at the equator (300–500 ppm, or 400±100 ppm) represents deep atmospheric NH_3, the corresponding $NH_3/H = 2.27\pm0.6\times10^{-4}$.

(l) Briggs and Sackett (1989), using the VLA and the Arecibo microwave and radio data. The authors reported 10× solar H_2S, using solar $S/H = 1.88\times10^{-5}$ from then current listing (Cameron 1982). The S/H result is questionable (see text).

(m) Protosolar values based on present-day solar photospheric values of Lodders et al. (2009, table 4). The proto-solar abundances are calculated from the present-day values using the following corrections: +0.061 dex for He and +0.053 dex for all other elements.

troposphere, but the extent of such depletion will continue to be a subject of debate until precise in situ measurements can be made. In this regard, the final proximal orbits of Cassini in September 2017 are promising for the measurement of helium by the Ion and Neutral Mass Spectrometer down to ~1700 km or ≤0.1 nanobar (S. Edgington, personal comm., 2015), which is above Saturn's homopause level (1000–1100 km, or ~10–100 nanobar; Atreya 1986; Strobel et al., this book), and perhaps deeper in the final trajectory when the spacecraft plunges into Saturn. Extrapolation to a well-mixed troposphere would be model dependent even if the homopause level could be derived independently from the Cassini occultation data in the proximal orbits. Hence, precise helium abundance measurement directly in the well-mixed troposphere will still be essential, and that can only be done from an entry probe.

The nitrogen elemental abundance in Saturn is obtained from Saturn's principal nitrogen-bearing molecule, NH_3. From an analysis of the Cassini Visual and Infrared Mapping Spectrometer (VIMS) data, Fletcher et al. (2011) derive an ammonia mole fraction, $f NH_3$, in the 1–3 bar region that is 140±50 ppm (scattering), 200±80 ppm (non-scattering), and rising to 300–500 ppm at the equator. If we assume that maximum in ammonia measured at the equator (300–500 ppm, taken as $4\pm1\times10^{-4}$ here) represents also the NH_3 mole fraction in Saturn's deep well-mixed troposphere, then the corresponding $NH_3/H = 2.27\pm0.6\times10^{-4}$. That would imply an N/H enrichment of about 3× solar at Saturn, in contrast to Jupiter's roughly 3–5× solar. Previously, de Pater and Massie (1985) also found a 3× solar enhancement in Saturn's N/H in the 3-bar region, based on the VLA observations. The VLA and the Cassini RADAR 2.2 cm data (Laraia et al. 2013) also show that ammonia is subsaturated down to several bars, which most likely results from the loss of NH_3 in the lower clouds of NH_4SH (or another form such as $(NH_4)_2S$) at ≥5 bars and the NH_3-H_2O (aqueous-ammonia) solution cloud between approximately 10 and 20 bars, depending on the enhancement of O/H (H_2O) above solar (Atreya et al. 1999; Atreya and Wong 2005; see also Section 2.6 and Figure 2.9 therein). Whether the above 3× solar N/H in the 3-bar region is representative of the true nitrogen elemental ratio in Saturn's deep well-mixed troposphere is presently an open question, as the infrared or radio data can neither confirm it nor rule it out. Unlike Saturn, there is no such ambiguity in the determination of Jupiter's N/H, since direct in situ measurements of NH_3 could be made by the Galileo probe mass spectrometer (GPMS; Niemann et al. 1998) down to 21 bars, which is well below the expected NH_3 condensation level of 0.5–1 bar. Independently, NH_3 was derived also by analyzing the attenuation of the Galileo probe-to-orbiter radio communication signal (L-band at 1387 MHz or 21.6 cm) by ammonia in Jupiter's atmosphere (Folkner et al. 1998). NH_3 from the two sets of data agree to within 20%, with tighter constraints coming from the radio attenuation data, which yields N/H = 5.40±0.68× solar (Table 2.1). It is generally assumed the Galileo probe value is likely representative of the global N/H in Jupiter, as the measurements were done well below any possible traps of ammonia, including condensation clouds of NH_3, NH_4SH, and NH_3-H_2O. Preliminary deep NH_3 values from the Juno microwave radiometer (Bolton et al. 2017) overlap the Galileo mass spectrometer value within the range of uncertainty of the two datasets, but not the Galileo radio attenuation data (Table 2.1). At Saturn, NH_3 from remote sensing extends to ~3 bars; however, an entry probe to deeper levels can answer whether that value is representative of the global well-mixed N/H or similar to C/H.

Sulfur is sequestered largely in the H_2S gas in the atmospheres of Jupiter and Saturn. Whereas Jupiter's H_2S could be measured directly and precisely in situ by the Galileo probe (Table 2.1), it was derived indirectly at Saturn by fitting the VLA and Arecibo microwave and radio data to assumed NH_3 abundances (Briggs and Sackett 1989). Although direct microwave absorption by H_2S could not be measured in these observations, they deduced H_2S by analyzing NH_3, whose abundance is controlled to some extent by H_2S, since models predict it would remove a portion of the NH_3 vapor via the formation of an NH_4SH cloud below. Using the then-available solar $S/H=1.88\times10^{-5}$ (Cameron 1982), they derived a 10× solar enrichment of S/H in Saturn's atmosphere, which translates into 12–13× solar S/H using current solar S/H values, or about four times the value determined by the Galileo probe in Jupiter (Table 2.1). It is important to add a caveat, however. Whereas the Jupiter result comes from direct, in situ

measurement of H_2S, the above result for Saturn is highly model-dependent, as it depends on the assumption of the formation of purported NH_4SH cloud whose thermochemical properties are poorly constrained. Since sulfur is a key heavy element in the models of Saturn's formation, a fresh set of data on Saturn's H_2S is warranted.

We list P/H in Table 2.1, but add a caveat that it may not represent the true P/H value in the deep well-mixed atmospheres of Jupiter or Saturn. This is because PH_3, the principal reservoir of phosphorus in the atmospheres of Jupiter and Saturn, is a disequilibrium species that is thermochemically stable in the deep atmosphere at pressures of about one thousand bars where the temperature is ~1000 K or greater (Fegley and Prinn 1985; Visscher and Fegley 2005), but it could only be measured in the upper troposphere/lower stratosphere. As PH_3 is dredged up from deep in the atmosphere to the upper atmosphere, it may potentially undergo loss due to oxidation to P_4O_6 by water vapor and solution in any water clouds along the way, or by other chemical reactions. Thus, the P/H ratio deduced from observations of PH_3 for Saturn and Jupiter in the upper atmosphere may represent a lower limit to the P/H ratio in their deep well-mixed atmosphere. Hence, the P/H values listed in Table 2.1 should not automatically be taken as a good proxy for the enrichment of other heavy elements not yet measured in Jupiter or Saturn. On the other hand, disequilibrium species such as PH_3, GeH_4, AsH_3, and CO are excellent tracers of the strength of convective mixing in the deep atmospheres of Saturn and Jupiter, and some could potentially be exploited to yield also a rough estimate of the deep water abundance.

Oxygen is arguably the most crucial of all heavy elements for constraining the formation models of Jupiter and Saturn. This is because in the reducing environments of the giant planets, oxygen is predominantly sequestered in water, which was presumably the original carrier of the heavy elements that formed the core and made it possible to accrete gas and complete the planet formation. (CO is another oxygen bearing species, but is a million times less abundant than water.) Yet the deep well-mixed abundance of water, and hence of O/H, remains a mystery. In the case of Jupiter, the Galileo probe entered an anomalously dry region known as a 5-micron hot spot. In this "Sahara Desert of Jupiter," water was found to be severely depleted (Niemann et al. 1998; Atreya et al. 1999, 2003). Although the probe mass spectrometer measured water vapor down to 21 bars, i.e. well below the expected condensation level of H_2O between 5 and 10 bars, it was still sub-solar at that level (Table 2.1), but rising. The determination of Jupiter's water abundance must await the analysis of Juno microwave radiometer observations in 2016–2017. No measurements of water vapor are available for Saturn's troposphere, however. The presence of water in Saturn's atmosphere is inferred indirectly from observations of visible lightning by Cassini's imaging spectrometer where lightning storms were predicted by Cassini's radio observations (Dyudina et al. 2010). Broadband clear filter observations showed visible lightning at ~35°S on the nightside in 2009 (Dyudina et al. 2010) and in blue wavelengths only on the dayside in the 2010–2011 giant lightning storm at ~35°N (Dyudina et al. 2013). These authors conjecture that a 5- to 10-times enhancement of water over solar can explain Saturn's lower occurrence rate for moist convection, an indicator of lightning, compared to Jupiter's (Dyudina et al. 2010). Similarly, using thermodynamic arguments Li and Ingersoll (2015) conclude that Saturn's quasi-periodic giant storms, which recur every few decades, result from interaction between moist convection and radiative cooling above the water cloud base, provided that the tropospheric water vapor abundance is 1 or greater, i.e. O/H $\geq$10× solar. Such an enrichment in O/H would result in a droplet cloud of NH_3-H_2O at ~20-bar level at Saturn (Atreya and Wong 2005; see also section 2.6 and figure 2.9 therein). Although direct measurements of Saturn's well-mixed water may have to wait for future missions, as discussed in Section 2.5, the recent discoveries of hot giant exoplanets and a Saturn-analog exoplanet are making it possible to measure H_2O abundances in their atmospheres, and in turn informing possible H_2O abundances in solar system giant planets.

Highly precise measurements of methane in the atmosphere of Saturn have been carried out with Cassini's composite infrared spectrometer (CIRS) instrument (Flasar et al. 2005), which yield a mole fraction of $CH_4 = 4.7\pm0.2\times10^{-3}$ (Fletcher et al. 2009b). This results in a robust determination of the C/H ratio in Saturn (about twice the Jupiter value) that can be compared with rather imprecise but definitely

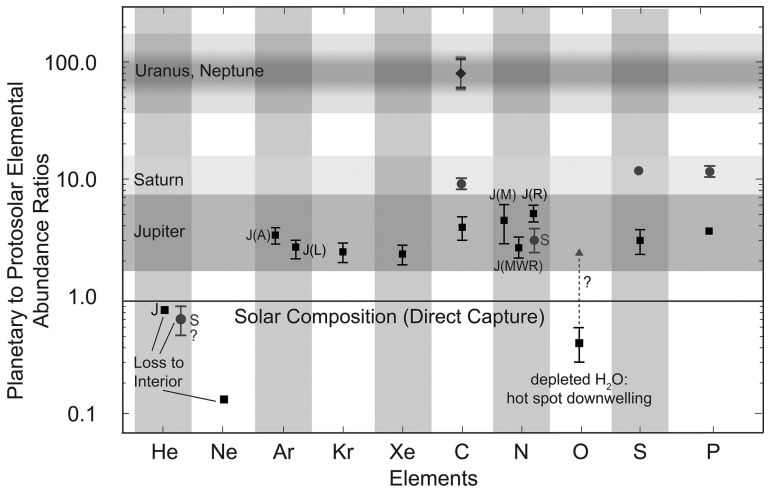

Figure 2.1 Abundances of key elements in the atmospheres of Saturn (brown dots, and label S) and Jupiter (black squares) relative to protosolar values derived from the present-day photospheric values of Asplund et al. (2009). Only C/H is presently determined for Uranus and Neptune, though poorly; its best estimate from Earth-based observations is shown. The values are listed in Table 2.1. All values are ratioed to H (multiply by 2 for ratio to H_2). Direct gravitational capture would result in solar composition, i.e. no volatile enrichment, hence they would all fall on the horizontal line (normalized to solar) in the middle of the figure. Only He, C, N, S, and P have been determined for Saturn, but only C/H is robust for the well-mixed atmosphere (see text). The Jupiter values are from the Galileo probe mass spectrometer (GPMS), except for N/H from NH_3 that was measured on the Galileo probe by the GPMS [J(M)] and from attenuation of the probe radio signal through the atmosphere [J(R)] as well as Juno microwave radiometer [J(MWR)], whose preliminary result is shown. For Ar, enrichments using both Asplund et al. [J(A)] and Lodders et al. [J(L)] solar values are shown. O/H is sub-solar in the very dry entry site of the Galileo Probe at Jupiter, but was still on the rise at the deepest level probed. Helium is depleted in the shallow troposphere due to condensation and differentiation in the planetary interior. Ne was also depleted in Jupiter as neon vapor dissolves in helium droplets. (A black-and-white version of this figure appears in some formats. For the color version, please refer to the plate section.)

higher estimates of C/H in Uranus and Neptune, as a way of constraining the giant planet formation scenarios.

Heavy noble gases, Ne, Ar, Kr, and Xe, have been measured only in Jupiter's atmosphere (Table 2.1), since they can only be detected in situ by an entry probe, not by remote sensing. As noble gases are chemically inert, their abundance is unaffected by chemistry and condensation processes that control NH_3, H_2S, H_2O, and PH_3. Thus, the heavy noble gas enrichments are expected to be the same everywhere in the atmosphere. At Jupiter, with the exception of neon, they range from a factor of 2 to 3× solar within the range of uncertainty of their planetary measurements and the solar values (Table 2.1). As neon dissolves in liquid helium, it is removed along with helium, which condenses in the 3 megabar region in Jupiter's interior, and is thus found depleted at observable shallow tropospheric levels (Wilson and Militzer 2010). At Saturn, neon is expected to meet the same fate.

Figure 2.1 shows the enrichment factors of the heavy elements and He in the atmospheres of Saturn and Jupiter relative to their protosolar values (all ratioed to H). Here we use the Asplund et al. (2009) compilation of photospheric elemental abundances (their table 1), as they represent an improvement over previous conventional standards (e.g. Anders and Grevesse 1989; Grevesse et al. 2005, 2007) and result from the use of a 3D hydrodynamic model of the solar atmosphere, nonlocal thermodynamic equilibrium effects, and improved atomic and molecular data. The photospheric values are then converted to protosolar elemental abundance (see table footnote). The latter account for the effects of diffusion at the bottom of the convective zone on the chemical composition of the photosphere, together with the effects of gravitational settling and radiative accelerations. According to Asplund et al. (2009), the protosolar metal abundances relative to hydrogen can be obtained from the present-day values increased by +0.04 dex, i.e. ~11%, with an uncertainty of ±0.01 dex; the effect of diffusion on He is very slightly larger: +0.05 dex (±0.01) (dex stands for "decimal exponent," so that 1 dex=10; it is a commonly used

unit in astrophysics). Lodders et al. (2009) suggest a slightly larger correction of +0.061 dex for He and +0.053 dex for all other elements. Previously, Grevesse et al. (2005, 2007) used the same protosolar correction of +0.05 dex for all elements.

Figure 2.1 is based on protosolar correction to Asplund et al. (2009) photospheric abundances, while Table 2.1 lists planetary elemental enrichment factors also for Lodders et al. (2009) protosolar values. Whereas the difference between the enrichment factors based on Asplund et al. and Lodders et al. values is at most 10 to 15% for most elements, Asplund et al. estimate nearly 30% greater enrichment for Ar/H, compared to Lodders et al. (Table 2.1).

The difference in Jupiter's Ar enrichment factors based on Asplund et al. (2009) and Lodders et al. (2009) can be traced back largely to the choice of O/H employed by the two sets of authors. Because of their high excitation potentials, noble gases do not have photospheric spectral features; hence their solar abundances are derived indirectly. Asplund et al. (2009) infer solar Ar/H following the same procedure as Lodders (2008), i.e. by using, amongst other things, the Ar/O data from the solar wind, solar flares, and solar energetic particles, but employing their own photospheric abundances of O/H that have a somewhat lower uncertainty than Lodders et al. (2009). This accounts for much of the abovementioned 30% difference in Jupiter's Ar/H enrichment factor. Nevertheless, within the range of uncertainty of Jupiter's Ar abundance and the dispersion in the solar values, the Ar/H enrichment in Jupiter relative to the solar Ar/H is nearly the same whether one uses Asplund et al. (2009) or Lodders et al. (2009) solar Ar/H. We show both results in Figure 2.1. A word of caution about oxygen, which is used by the above authors as a proxy for deriving the solar Ar/H, is in order, however, as explained below.

Ever since concerted efforts were made to determine the solar elemental abundances, particular attention has been paid to oxygen, as oxygen is the most abundant element that was not created in the Big Bang, and third only to H and He, which were created in the Big Bang. Furthermore, the principal reservoir of oxygen in Saturn and Jupiter, H_2O, was presumably the original carrier of the heavy elements to these planets. Thus, oxygen is centrally important to the question of origin of all things. Yet, its abundance in the sun has been revised constantly. As illustrated in Figure 2.2, the solar O/H values have gyrated up and down several times in the past four decades, starting with the classic work of Cameron (1973) to the present. The highest solar O/H value is the one recommended by Anders and Grevesse (1989), which remained the standard for a good fifteen years, only to be revised downward by nearly a factor of two in 2005 (Grevesse et al. 2005), and having crept up a bit since then. Not surprisingly, the solar Ar/H, also plotted in Figure 2.2, shows the same trend as O/H over time, though they are not completely proportional to each other, nor are they expected to be. Thus, one needs to be vigilant about changes in the photospheric abundance of oxygen and other elements such as argon that use oxygen as a reference.

In summary, the most robust elemental abundance determined to date in Saturn is that of carbon. At 9× solar, Saturn's C/H is a little over twice the C/H ratio in Jupiter. This is consistent with the core accretion model of giant planet formation, according to which progressively increasing elemental abundance ratios are expected from Jupiter to Neptune. Carbon is the only heavy element ever determined for all four giant planets (Figure 2.1), and indeed it is found to increase from 4× solar in Jupiter to 9× solar in Saturn, rising to 80(±20)× solar or greater in both Uranus (Sromovsky et al. 2011; E. Karkoschka and K. Baines personal communication, 2015) and Neptune (Karkoschka and Tomasko 2011), using the current solar C/H from Table 2.1. The same trend is also seen in the S/H ratio of Saturn compared to Jupiter, except for a fourfold increase from Jupiter to Saturn, but Saturn's S/H is less secure, as discussed above. The difference in the relative changes of C/H and S/H is worth noting, but caution should be exercised to not overinterpret it. This is because H_2S is a thermochemically condensible volatile in the gas giants, unlike CH_4. Saturn's S/H would benefit greatly from a fresh set of modern data. A similar fourfold increase is also seen in the P/H ratio in Saturn compared to that in Jupiter, and the relative change may be valid if the disequilibrium species PH_3 meets a similar fate in the tropospheres of Saturn and Jupiter. On the other hand, the observed 3× solar N/H ratio in Saturn seems puzzling, as it is about a factor of two less, not more, than Jupiter's N/H, contrary to the predictions of conventional formation models. However, the

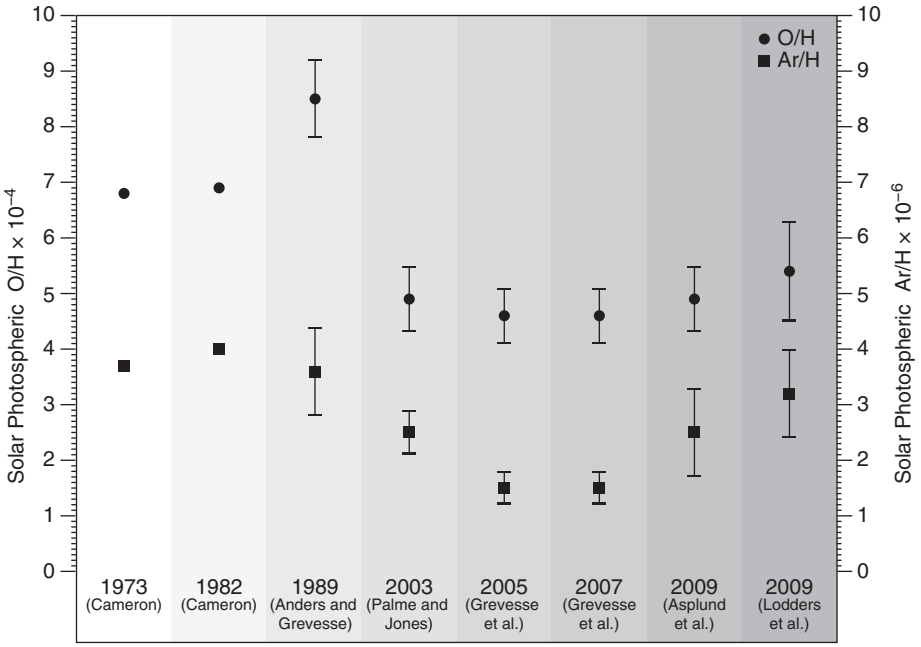

Figure 2.2 Time history of the solar photospheric O/H and Ar/H, showing only the major milestones. Although Ar/H shows the same trend as O/H, they do not track each other exactly. The solar photospheric values for O/H ($\times 10^{-4}$) and Ar/H ($\times 10^{-6}$) plotted here are, respectively, 6.8 and 3.7 (Cameron 1973), 6.9 and 4 (Cameron 1982), 8.5±0.7 and 3.6±0.8 (Anders and Grevesse 1989), 4.9±0.6 and 2.5±0.4 (Palme and Jones 2003), 4.6±0.5 and 1.5±0.3 (Grevesse et al. 2005, 2007), 4.9±0.6 and 2.5±0.8 (Asplund et al. 2009), and 5.4±0.9 and 3.2±0.8 (Lodders et al. 2009).

present data on Saturn's NH_3 in the 3 bar region do not rule out much greater ammonia abundance in the deep well-mixed atmosphere of Saturn, as discussed earlier. Presence of water is inferred in Saturn's troposphere indirectly from localized lightning observations, but no firm conclusions can be drawn from it on the global O/H ratio in Saturn. The Juno spacecraft is designed to measure and map water to several hundred bars in Jupiter's troposphere, which will provide a definitive answer on Jupiter's O/H ratio. In Jupiter at least, for which data are available for most of the heavy elements, except for O/H, it is striking that the heavy noble gases Ar, Kr, and Xe all display similar enrichment over solar by a factor of 2 to 3 (or, 2 to 2.5 with Lodders' solar values, Table 2.1), whereas enrichment of non-noble gas elements, carbon, nitrogen, and sulfur, is greater, ranging from 4 to 6. (Regarding S/H, from their clathrate hydrate model, Gautier et al. (2001) calculate an S/H enrichment in Jupiter that is twice the value measured by the Galileo probe (Table 2.1), or ~6× solar, and attribute the lower measured value to the loss of H_2S in troilite (FeS) in the inner solar nebula.) Though it may seem tempting and convenient to lump them all together and suggest that the heavy elements in Jupiter are enriched uniformly by a factor of 4±2 relative to their solar abundances, we advise caution.

The differences between the enrichments of the heavy noble gases and those of the non-noble gas heavy elements are apparently real, and may indicate two distinct populations arising from differences in the way noble gases were delivered (see also Section 2.4.3). Robust measurements of the same set of heavy elements at Saturn as at Jupiter are crucial to determining whether they have solar composition, as proposed by Owen and Encrenaz (2006), which will in turn have a bearing on the models of the origin, nature, and delivery of the Saturn-forming planetesimals. Similar efforts are now underway to measure key elemental abundances, particularly of O and C, in the atmospheres of giant exoplanets, and in using them to constrain formation conditions of exoplanetary systems (see Section 2.5).

2.2.2 Isotopic Composition of Saturn's Atmosphere and Comparison to Jupiter

Isotope ratios provide an insight into the conditions prevailing at the time of formation of the solar system and even early in the beginning of the universe. The giant planets and the terrestrial planets formed from much of the same initial inventory of material in the primordial solar nebula. Thus, the stable gas isotope ratios originally were the same in all planets. Abiotic fractionation of isotopes can occur due to escape of gases to space, loss to surface, phase change, or photochemistry. Indeed, fractionation of various stable gas isotopes has been found in the atmospheres of comparatively small solar system objects including Venus, Earth, Mars, and Titan (e.g. von Zahn et al. 1983; Niemann et al. 2010; Atreya et al. 2013; Webster et al. 2013; Mahaffy et al. 2014), and has been attributed mainly to the loss of their volatiles to space over geologic time. On the other hand, the sheer mass of the giant planets, in particular Jupiter and Saturn, does not permit loss of volatiles either by thermal, charged particle or other processes, hence their original isotopic ratios of elements are expected to be preserved, for all practical purposes. Thus, their present atmospheric isotope ratios should, in theory, also represent protosolar values.

Only a handful of the isotopes have been measured in Saturn's atmosphere: $^{13}C/^{12}C$, D/H, and an upper limit on $^{15}N/^{14}N$. In the atmosphere of Jupiter, $^{3}He/^{4}He$, $^{36}Ar/^{38}Ar$, and all isotopes of Xe except for ^{124}Xe and ^{126}Xe that together comprise 0.2% of total xenon in the sun have been measured, in addition to $^{13}C/^{12}C$, D/H, $^{15}N/^{14}N$. The measurement of noble gas isotopes in Jupiter was facilitated by in situ measurements with a mass spectrometer on the Galileo probe (GPMS). The isotope ratios for the atmosphere of Saturn and Jupiter are listed in Table 2.2. The helium, carbon, and xenon isotope ratios of Jupiter are nearly identical to the solar values, as expected.

The hydrogen isotope ratio, D/H, in Jupiter and Saturn is important for understanding the very beginnings of the universe and galactic evolution. Deuterium was formed following the Big Bang, but has been declining ever since because its destruction in the stars far outweighs any new creation. Thus, the D/H ratio in Jupiter and Saturn represents the protosolar value of D/H in the sun, in which it cannot be measured directly today. The value derived by the GPMS in Jupiter's atmosphere was thus the first measurement of the protosolar D/H ratio (Mahaffy et al. 1998). The result is in agreement with the D/H measurements done later with the short-wavelength spectrometer on the Infrared Space Observatory (ISO, Lellouch et al. 2001) and theoretical estimates (Table 2.2). This gives confidence in the D/H ratio measured by ISO in Saturn's atmosphere. Within the range of uncertainty, Saturn's D/H ratio is similar to that in Jupiter.

The nitrogen isotope ratio was measured in Jupiter's atmosphere by the Galileo probe mass spectrometer (Owen et al. 2001), and represented the first measurement of the protosolar $^{15}N/^{14}N$ ratio. The value in the sun is now available from the Genesis measurements (Marty et al. 2011) and is identical to the GPMS result for Jupiter. The ISO data give a slightly lower $^{15}N/^{14}N$, probably resulting from isotope fractionation below the ammonia clouds to which the ISO data apply. Note, however, that $^{15}N/^{14}N$ from ISO has large uncertainties that can easily envelop the GPMS result. Unlike Jupiter, only an upper limit on the $^{15}N/^{14}N$ ratio in Saturn's atmosphere is available. Using the Texas Echelon Cross Echelle Spectrograph (TEXES) on NASA's Infrared Telescope Facility (IRTF), Fletcher et al. (2014) observed spectral features of $^{14}NH_3$ and $^{15}NH_3$ in 900 cm^{-1} and 960 cm^{-1}, and derived an upper limit on the $^{15}N/^{14}N$ ratio of 2×10^{-3} for the 900 cm^{-1} channel and 2.8×10^{-3} for the 960 cm^{-1} channel. Though these values fall in the range of Jupiter's $^{15}N/^{14}N$ ratio, in the absence of actual measurement they represent only upper limits of $^{15}N/^{14}N$ in Saturn's atmosphere. In Figure 2.3, we show the best available data on this important ratio in the sun, interstellar medium, Jupiter, Saturn, and comets (from CN, HCN, and NH_2), which represent the original reservoirs of nitrogen (left panel, labeled "Primordial"), and in N_2 of the terrestrial planets and Titan, where nitrogen is secondary (right panel, labeled "Secondary"). The corresponding nitrogen isotope ratios are listed in Table 2.3. Nitrogen isotope fractionation is clearly evident in the terrestrial bodies. The lighter isotope floats up to the top of the atmosphere and escapes preferentially, leading to the build-up of the heavier isotope.

Table 2.2 *Elemental Isotopic Ratios in the Sun, Jupiter, and Saturn*

Elements	Sun	Jupiter	Saturn
$^{13}C/^{12}C$	0.0112[a]	0.0108±0.0005[i]	0.0109±0.001[o]
$^{15}N/^{14}N$	2.27±0.0810^{-3} [b]	(2.3±0.3)×10^{-3}	<2.0×10^{-3} [p]
		(0.8–2.8 bar)[j]	(900 cm^{-1} channel)
		1.9(+0.9, −1.0)×10^{-3}	<2.8×10^{-3} [p]
		(0.2–1.0 bar)[k]	(960 cm^{-1} channel)
$^{36}Ar/^{38}Ar$	5.5±0.0[c]	5.6±0.25[l]	
$^{136}Xe/Xe$	0.0795[a]	0.076±0.009[l]	
$^{134}Xe/Xe$	0.0979[a]	0.091±0.007[l]	
$^{132}Xe/Xe$	0.2651[a]	0.290±0.020[l]	
$^{131}Xe/Xe$	0.2169[a]	0.203±0.018[l]	
$^{130}Xe/Xe$	0.0438[a]	0.038±0.005[l]	
$^{129}Xe/Xe$	0.2725[a]	0.285±0.021[l]	
$^{128}Xe/Xe$	0.0220[a]	0.018±0.002[l]	
$^{20}Ne/^{22}Ne$	13.6[a]	13±2[l]	
$^{3}He/^{4}He$	1.66×10^{-4} [a]	(1.66±0.05)×10^{-4} [m]	
	(1.5±0.3)×10^{-4} (meteoritic)[d,e,f,g]		
D/H	(2.0±0.5)×10^{-5} [a]	(2.6±0.7)×10^{-5} [m]	1.7(+0.75, −0.45)×10^{-5} [n]
	(2.1±0.5)×10^{-5} [h]	(2.25±0.35)×10^{-5} [n]	
	protosolar values		

[a] Asplund et al. (2009), updated from Rosman and Taylor (1998);
[b] Marty et al. (2011), from Genesis;
[c] Vogel et al. (2011);
[d] Black (1972);
[e] Eberhardt (1974);
[f] Geiss and Reeves (1972);
[g] Geiss (1993);
[h] Geiss and Gloeckler (1998);
[i] Niemann et al. (1998);
[j] Owen et al. (2001), from Galileo probe mass spectrometer (GPMS) in situ measurements, largely below the NH_3 condensation level;
[k] Fouchet et al., (2000), from ISO infrared remote sensing measurements, largely above the NH_3 condensation level;
[l] Mahaffy et al. (2000), normalized to 1.0 for xenon isotopes measured, only ^{126}Xe and ^{124}Xe, which together make up 0.2% of the total xenon in the sun, could not be measured by the GPMS in Jupiter, and the xenon error bars are with respect to the ratio of each isotope to its non-radiogenic terrestrial value;
[m] Mahaffy et al. (1998), from GPMS;
[n] Lellouch et al. (2001), from ISO;
[o] Fletcher et al. (2009b);
[p] Fletcher et al. (2014).

2.2.3 Saturn's Interior

Saturn's interior may be probed indirectly through models and the measurement of the planet's mean density and gravitational moments (Fortney et al., this book) and measurement of the planet's dissipation factor (e.g. Remus et al. 2012). It has long been known that it is mostly made of hydrogen and helium, except for the presence of a central dense core. Detailed models show that in spite of its low global density of 0.688 g/cm^3, Saturn must contain a significant fraction

Table 2.3 *Nitrogen Isotope Ratios in the Solar System*

Objects	$^{14}N/^{15}N$	$^{15}N/^{14}N$ ($\times10^{-3}$)
Sun (protosolar)[a]	441±5	2.27±0.03
Jupiter[b]	442±58	2.30±0.3
Saturn[c]	<357	<2.8
Interstellar medium (ISM)[d]	450±98	2.2±0.5
Comet Hale-Bopp (CN)[e]	140±30	7.1(+2.0, −1.3)
Comet Hale-Bopp (CN)[f]	140±35	7.1(+2.4, −1.4)
Comet Hale-Bopp (HCN)[g]	323±46	3.1(+0.5, −0.4)
Comet Hale-Bopp (HCN)[f]	205±70	4.9(+2.5, −1.3)
Comet Holmes (CN)[f]	139±26	7.2(+1.7, −1.1)
Comet Holmes (HCN)[f]	165±40	6.1(+1.9, −1.2)
Comets (NH_2)[h]	80–190	5.26–12.5
Earth	272	3.68
Venus[i]	272±54	3.7(+0.9, −0.6)
Mars (atmosphere)[j]	173±11	5.8±0.4
Mars (solid body)[k]	276.5±0.25	3.62
Titan[l]	167.7±0.6	6.0±0.02

[a] Marty et al. (2011), from Genesis sample analysis;
[b] Owen et al. (2001), Galileo probe mass spectrometer;
[c] Fletcher et al. (2014), IRTF;
[d] Dahmen et al. (1995);
[e] Arpigny et al. (2003);
[f] Bockelée-Morvan et al. (2008);
[g] Jewitt et al. (1997);
[h] Rousselot et al. (2014), derived from emission lines of NH_2 in twelve comets between 2002 and 2013, and the authors state that the range in $^{14}N/^{15}N$ is probably more appropriate to use than the average value of 127, which does not account for uncertainties because of the difficulty in accurately subtracting the solar continuum for each region of interest;
[i] Hoffman et al. (1979), Pioneer Venus;
[j] Wong et al. (2013), from MSL;
[k] Matthew and Marti (2001), from the oldest known Martian meteorite, ALH84001 (4.1 Gyr old);
[l] Niemann et al. (2010), Huygens-GCMS.

of its mass as heavy elements: between about 12 and 28 M_E (Nettelmann et al. 2013; Helled and Guillot 2013), corresponding to a mass fraction Z=0.13 to 0.29 or a global enrichment in heavy elements of 8.9 to 20 times the solar value.

In classical three-layer models, most of the heavy elements are embedded in a central core. The solutions of Helled and Guillot (2013), assuming a well-defined central core and a homogeneous abundance of heavy elements in the envelope, indicate a core with a mass between 10 and 20 M_E and an envelope with 4 to 8 M_E of heavy elements, corresponding to an enrichment of 4 to 8 times the solar value. The abundances of C-, N-, and S-bearing species in the atmosphere account for the lower limit of this range, meaning that the elusive O can be enriched only as much as C. As the "total" enrichment in heavy elements is constrained by the interior models, the addition of other species (e.g. silicates) into the envelope would mean less enrichment for others, which would make O even less enriched, implying a C/O ratio that is very likely to be supersolar in Saturn's atmosphere. Solutions by Nettelmann et al. (2013) add one degree of freedom, the possibility for the abundance of heavy elements to vary in the envelope. That leads to the possibility of even smaller core masses, but with a deep envelope that is enriched in heavy

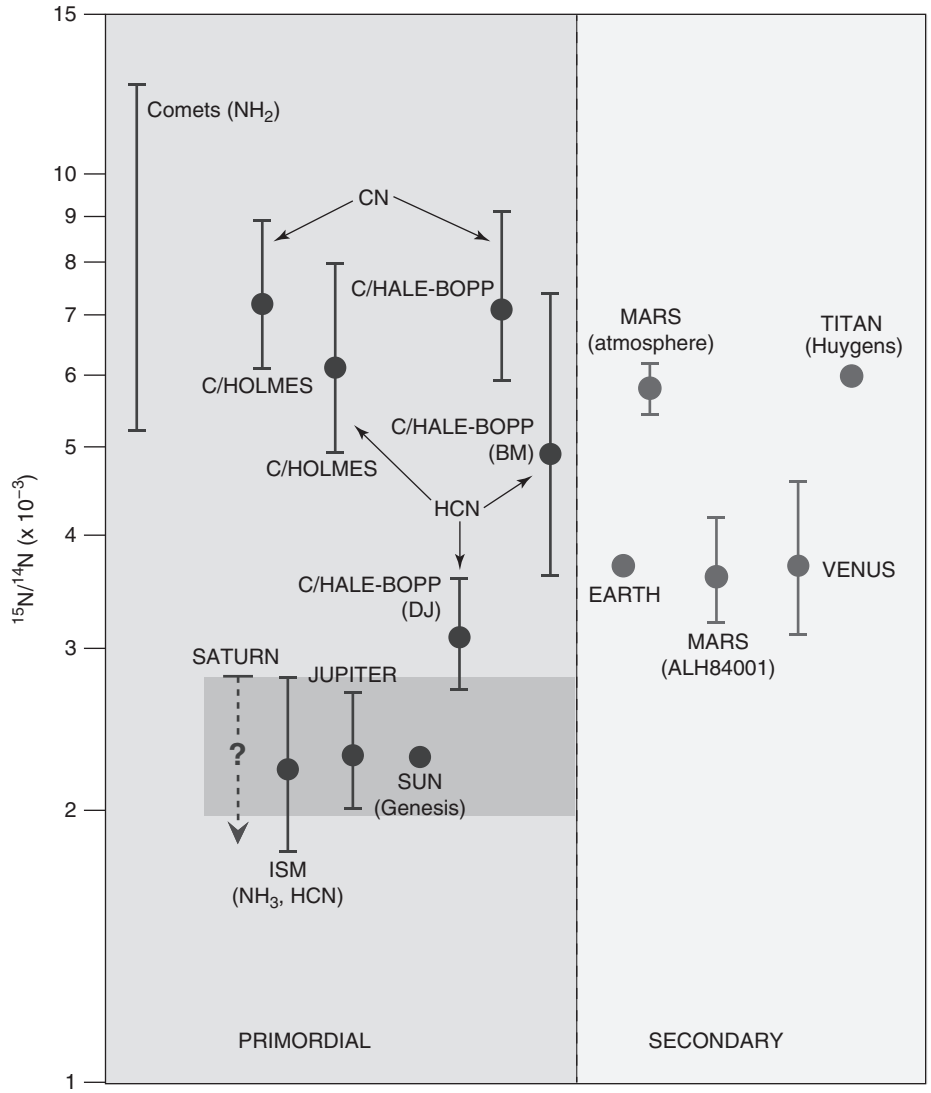

Figure 2.3 A comparison of the current nitrogen isotope ratios in primordial (sun, ISM, Jupiter, Saturn, and comets; left panel) and secondary (Venus, Earth, Mars, and Titan; right panel) reservoirs. The values for the secondary reservoirs illustrate loss of nitrogen from these objects over geologic time. A subset of the $^{15}N/^{14}N$ ratios based on then available data can be found in Owen et al. (2001) and Atreya et al. (2009). References for current ratios are listed in Table 2.3. For Mars, the value in ALH84001 is also shown, and represents $^{15}N/^{14}N$ for solid Mars, which is nearly the same as for the atmosphere of Earth, as expected, considering that these planets presumably acquired their original building material from the same source. The substantially higher $^{15}N/^{14}N$ in Mars atmosphere today compared to Earth's atmosphere is the consequence of thermal- and solar–wind-induced escape of nitrogen from (lighter and non-magnetic) Mars over geologic time. Higher $^{15}N/^{14}N$ in Titan's present atmosphere compared to Earth's atmosphere may reflect the value in its building blocks, coupled with atmospheric loss over time. In comets, a similar value of $^{15}N/^{14}N$ has been measured in CN of a dozen comets, and in CN and HCN of comets Hale Bopp and Holmes. However, the $^{15}N/^{14}N$ in HCN in the latter two comets is substantially different from that in CN, and different observers (BM: Bockelée-Morvan et al. 2008, DJ: Jewitt et al. 1997) report different values, though all have large error bars. $^{15}N/^{14}N$ from NH_2 in a number of comets (Rousselot et al. 2014) is shown as a range, which is more appropriate than an average value because of the difficulty of accounting for solar continuum for each emission feature of NH_2, according to the authors. The reader is referred to Atreya et al. (2009) for additional discussion on the cometary $^{15}N/^{14}N$ and implications for Titan. For Saturn only upper limits from 900 cm^{-1} and 960 cm^{-1} spectral channels are available. Parts of this figure are taken from Figure 7.2 of Atreya et al. (2009), with permission from Springer. (A black-and-white version of this figure appears in some formats. For the color version, please refer to the plate section.)

elements. Thus, the picture that emerges is one in which a core is either well-defined or only partially mixed with the envelope, and the envelope is significantly enriched in heavy elements, but not in the same way for all species. Accounting for material that may be partially mixed in the deep envelope, Saturn's core appears to have a mass that is consistent with that required by core-accretion models (e.g. Ikoma et al. 2001). The enrichment of the envelope is to be explained either by planetesimal impacts or by upward mixing and/or core erosion. The former is traditionally difficult because the cross-section of a mature giant planet (i.e. when the planet has accreted its full mass and does not possess a circumplanetary disk anymore) is small. For example, simulations of impacts during the great heavy bombardment indicate that of an initial disk mass of 35 M_E, only between 0.05 and 0.1 M_E hit Saturn (the values are about double for Jupiter, due to a larger focusing factor; Matter et al. 2009).

Core erosion is made possible from a physical point of view because of the miscibility of species in metallic hydrogen (Wilson and Militzer 2010, 2012). However, while it is effective at Jupiter, Saturn's smaller envelope implies that only about 2 M_E may be mixed upward from a massive central core, assuming a 10% efficiency of the process (Guillot et al. 2004). A higher efficiency, or, more likely, the upward mixing of an initially heavy-element-rich primordial envelope, could explain the planet's heavy-element-rich atmosphere. Variations in the elemental composition (such as those leading to a supersolar C/O ratio) could be explained by a selective retention of species (e.g. silicates, water) in the deeper regions.

2.3 Saturn's Formation: Hydrodynamical Point of View

Standard models of Saturn's interior with a core surrounded by a hydrogen-helium envelope that is enriched in heavy elements fits well with the picture of its formation by core accretion followed by the capture of the gas envelope from the protoplanetary disk. However, considerable uncertainties remain, both on the internal structure itself and on formation models. To understand the end-to-end origin and evolution of Saturn, it is important to consider, then, the starting protosolar disk, the manner of formation and growth of the core, Saturn's circumplanetary disk, and any insight from the moons and rings. This section discusses each of these aspects from a hydrodynamical point of view.

2.3.1 Birth and Evolution of the Protosolar Disk

Any model of Saturn formation must begin with the protoplanetary disk, or solar nebula, from which the gas and dust of Saturn were derived. Constraints on giant planet formation include the disk lifetime, elemental composition (specifically, C/H, O/H, etc.,), and the overall mass of the disk. A low-opacity massive disk may fragment very early due to disk instability, but we argued in Section 2.1 that the overall architecture of our solar system does not match such an event. Core accretion, then, is constrained to build Saturn within a plausible disk lifetime. The model of Dodson-Robinson et al. (2008) provides a particular example of the detailed specification of a solar nebula model needed to build Saturn in an acceptably short length of time.

2.3.2 Formation and Growth of Giant Planet Cores

Core Formation

In the framework of the core accretion model, the first step is obviously to form a 10-Earth-masses core. In the classical view, gravity is the dominant process, and kilometer-sized planetesimals merge when they collide. In the end, a population of so-called "oligarchs" is produced, which accrete all the planetesimals within reach of their orbit (Kokubo and Ida 1998). Their mass is then typically $0.05(r/1AU)^{0.75}$ M_E.

Another model suggests that centimeter-sized dust aggregates are concentrated by vortices in the gas up to the point where the concentration of solids becomes gravitationally unstable, leading possibly directly to the formation of solid bodies of hundreds of kilometers (Johansen et al. 2007; see Turner et al. 2014a for a review of turbulent processes).

It has been shown recently that such embryos are very efficient at accreting pebbles, i.e. cm-sized aggregates moderately coupled to the gas (Lambrechts and Johansen 2012; Morbidelli and Nesvorny 2012). As such pebbles drift radially, nothing stops this growth, whose rate is exponential. Pebble accretion is to date the most promising mechanism to form a few-Earth-masses core within the lifetime of a protoplanetary

disk. Furthermore, Lambrechts et al. (2014) show that pebble accretion naturally stops when the core becomes massive enough to carve a dip in the gas that stops the radial drift of pebbles (~20 M_E). The end of the accretion of solids by the core then triggers the onset of the runaway accretion of gas.

Planet Migration

Cores and planets interact gravitationally with the gas disk. This leads to exchanges of energy and angular momentum, hence to a variation of the orbit of the planet. This is called planetary migration. Bodies of less than roughly 50 M_E do not perturb the gas profile much and are in the type I migration regime (Ward 1997). It has been shown in the last decade that type I migration can be directed inwards or outwards, depending on the thermodynamics of the gas disk (Paardekooper and Mellama 2006; Paardekooper et al. 2010, 2011). Typically, migration would be directed inwards in the outer, optically thin regions of the disk, while it can be directed outwards in the inner, optically thick regions. This opens the possibility of convergent migration towards a zero-torque migration radius where bodies of few Earth masses should gather, and hopefully merge (Lyra et al. 2010; Cossou et al. 2013). In general, there are two such radii, and their locations depend on the disk structure (Bitsch et al. 2013). One is inside the snowline and vanishes when the accretion rate in the disk decreases, and one is beyond the snowline, moving from roughly 10 AU to 4 AU as the disk ages (Bitsch et al. 2014). In any case, this new vision of planet migration (see Baruteau et al. 2014 for a recent and complete review) opens the possibility to keep the core of a giant planet safe at the zero-torque migration radius, instead of losing it into the star. It can then grow by slowly accreting its gas envelope.

When it is massive enough, the planet will open a gap in the gas disk (Papaloizou and Lin 1984; Crida et al. 2006), and thereby leave the type I migration regime. Planets opening gaps are in the type II, slower mode of migration, in which they follow roughly the viscous evolution of the disk (Lin and Papaloizou 1986; Crida and Morbidelli 2007; Dürmann and Kley 2015).

It should be noted that the migration of the Jupiter-Saturn pair is, however, more complex than that of a single giant planet. Jupiter and Saturn most likely enter in mean motion resonance, which can reverse their migration (Masset and Snellgrove 2001). A fine tuning of the disk parameters allows the Jupiter and Saturn pair to avoid any significant migration in the protosolar nebula (Morbidelli and Crida 2007). Another possibility is that Jupiter grew and migrated inwards first, then was caught up by Saturn, which made the pair migrate back outwards (Walsh et al. 2011). In this so-called "Grand Tack" scenario, the main asteroid belt is satisfactorily reproduced, and Jupiter's excursion sculpts the inner disk of embryos and planetesimals in a very favorable way for the formation of the terrestrial planets. It implies that Saturn came as close as about 2 AU from the Sun. Little room is left for gas accretion in this scenario, as the final masses of Jupiter and Saturn are ideal for such a tack, but Saturn could have been half its present mass, gaining the rest on the way out.

In any case, an unavoidable consequence of migration is that Saturn most likely was in resonance with Jupiter, on a circular orbit ~8 AU from the Sun, when the protosolar nebula dissipated. It reached its final orbit ~650 million years later, during a global dynamical instability among the giant planets, often referred to as the "Nice model" (Tsiganis et al. 2005).

2.3.3 Formation of Saturn and Its Circumplanetary Disk

As discussed above and illustrated in Figure 2.4, giant planets open gaps in the protoplanetary disk. The neighborhood of their orbit is depleted, splitting the disk into an inner and an outer disk. While the width of the gap is set solely by the Hill radius of the planet, the depth of the gap increases with the planet mass and is also a smooth function of the viscosity and aspect ratio of the disk (Crida et al. 2006). Even for massive planets like Saturn or Jupiter, the opening of the gap does not terminate gas accretion. Indeed, as can be seen in Figure 2.4, gas still flows towards the planet through the spiral wake. As a consequence, the final phase of runaway gas accretion corresponding to the collapse of the gas envelope (see Section 2.1) has no reason to end until a few Jupiter masses are reached. However, numerical simulations show that massive planets are capable of creating their own gas disk around them, inside the gap (Bate et al. 2003; Ayliffe and Bate 2012).

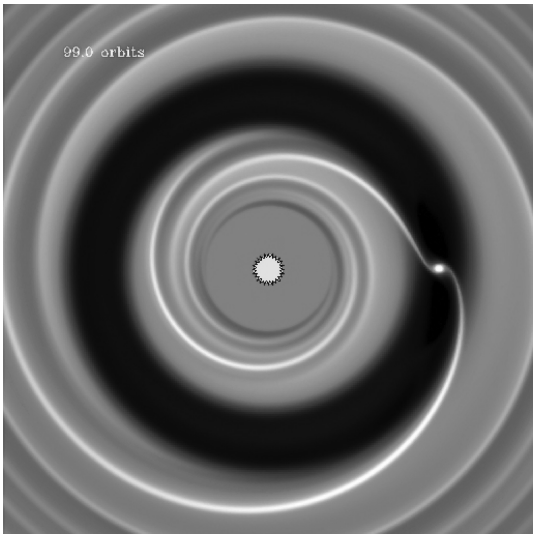

Figure 2.4 Gas density map from a 2D hydrodynamical simulation. Light color corresponds to high density, black to low density. The star is in the center of the image; the giant planet is on the right. The black annulus is the gap around the planetary orbit, and the white spot around the planet (not shown) is the CPD. (A black-and-white version of this figure appears in some formats. For the color version, please refer to the plate section.)

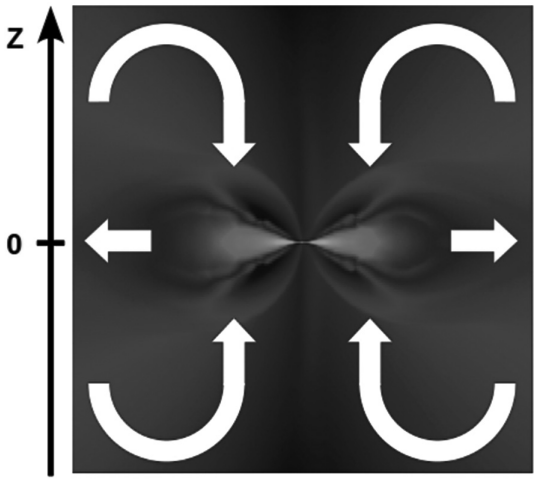

Figure 2.5 Vertical cut through the CPD of a Jupiter mass planet in a 3D simulation. The horizontal axis represents the distance to the star and the vertical axis is perpendicular to the orbital plane of the planet, with the planet in the center. The color corresponds to the gas density, and the arrows sketch the meridional circulation of the gas. (A black-and-white version of this figure appears in some formats. For the color version, please refer to the plate section.)

This circumplanetary disk (hereafter CPD) is poorly resolved in Figure 2.4, but has been studied in greater detail in other works.

The simulations reveal that the gas flow around a giant planet is 3D, and cannot be accurately modeled by a 2D simulation. Actually, most of the gas that reaches the CPD comes from a vertical direction, which is perpendicular to the orbital plane (Bate et al. 2003; Machida et al. 2008; Ayliffe and Bate 2009a,b; Tanigawa et al. 2012; Szulagyi et al. 2014). An explanation for this unexpected flow pattern is given by Morbidelli et al. (2014): in the upper layers of the disk the gravitational force from the planet is weaker, and therefore the gap tends to be narrower than in the midplane. Gas comes in, and being not supported by pressure, falls towards the midplane, where the planet ejects it back out of the gap, still in the midplane. Therefore, a meridional circulation pattern is created, as sketched by white arrows in Figure 2.5: gas ejected from the midplane by the planet expands vertically further away, and then slowly penetrates inside the gap from the upper layers, before falling back on the midplane. Note that such a full loop is much longer than an orbital period. Part of this vertical inflow falls on the CPD and the planet, contributing to the planet's growth.

This may have strong implications on the nature and rate of the solids in this flow. By the time a giant planet forms, dust is supposed to have sedimented in the midplane of the disk, being only stirred by turbulence. Micrometric grains, well coupled to the gas, should follow the gas flow, but larger aggregates may well be unable to reach the planet and its CPD.

In isothermal simulations (the only ones available so far in the literature), gas falls at a supersonic speed onto the CPD and shocks at the surface of the latter. In the absence of viscosity in the CPD, gas should in principle reach its centrifugal radius and orbit around the planet forever. This opens the possibility that the CPD acts as a bottleneck for planet growth, and limits the final mass of the giant planets (Rivier et al. 2012). There are good reasons to think that the CPD is really inviscid (Turner et al. 2010, 2014b; Fujii et al. 2011, 2014). Hence, Szulagyi et al. (2014) have measured the different sources of angular momentum loss in the CPD (torque from the central star, contact with the infalling gas), using mesh refinement around the planet in a 3D global simulation, allowing for the gap to form accurately. They deduce a mass-doubling time on the order of half a million years for a Jupiter-mass planet. This is much slower than the standard, 1D model of Pollack

et al. (1996), and could be the reason why Saturn, like most giant exoplanets (see section 2.5), did not grow more massive than Jupiter: depending when gas accretion starts, there is not enough time to grow super giant planets.

This type of research is demanding, both in terms of computing capability and time, hence it is still open. In particular, non-isothermal simulations are necessary to better determine the structure of the CPD. Its temperature has strong implications for the composition of the solids available to form the satellites and for the chemical species in the gas. Novel and promising results on gas accretion by a giant planet are expected in the future.

2.3.4 Formation of Saturn, from Consideration of the Formation of Moons and Rings

For a comprehensive understanding of the formation and evolution of Saturn, it is necessary also to gain an insight into the formation of Saturn's moons. Here we provide a brief discussion of this aspect of the Saturn system. About 60 satellites with confirmed orbits have been detected so far. Among them, 23 have quasi-circular orbits of radius smaller than 2 million kilometers in the plane of Saturn's equator: the so-called regular satellites. The others have eccentric, inclined (sometimes even retrograde), and larger orbits. They are called irregular satellites, and are supposedly captured. Hence, the irregular satellites do not inform much about Saturn's formation. In contrast, the rings and the regular satellites most likely formed together with Saturn in some way, and therefore provide constrains.

Titan, the largest moon of Saturn, dominates the population of satellites, being 60 times more massive than the second largest moon, Rhea. Titan's composition can provide further insight into the physico-chemical conditions prevailing in Saturn's CPD that must have played a crucial role in the make-up of Titan's building blocks. In situ measurements with the Huygens gas chromatograph mass spectrometer (Niemann et al. 2005, 2010) revealed for the first time that the bulk atmosphere of Titan is approximately 94% by volume nitrogen (N_2) and ~6% methane (CH_4). Methane may have originated on Titan, but direct external contribution is also possible. N_2, on the other hand, is almost certainly "secondary," i.e. instead of being delivered directly as N_2, it resulted from other nitrogen-bearing molecules originally captured in Titan's building blocks. Before nitrogen was actually detected on Titan by Voyager in 1980, Atreya et al. (1978) showed that the solar UV photolysis of ammonia (NH_3) could produce a substantial atmosphere of nitrogen on Titan in the past, which was eventually confirmed by Huygens in 2005. The dissociation of ammonia by impact shock heating has also been proposed (Jones and Lewis 1987; McKay et al. 1988; Sekine et al. 2011; Ishimaru et al. 2011). While it seems like an attractive hypothesis, it faces many hurdles, including the removal of accompanying copious oxygen-bearing species and hydrogen, not found on Titan (see, e.g. Atreya et al. 2009). The fact that Titan's N_2 is not primordial but formed from ammonia has important implications for Saturn's CPD, considering possible scenarios of Titan's formation. Similarly, the origin of Titan's methane has a bearing on Saturn's CPD, so it is also discussed here briefly.

Two possibilities for the origin of Titan's methane have been proposed: production on Titan, or delivery to Titan. In the former case, methane was produced by hydro-geochemistry, i.e. water-rock reactions or serpentinization in the interior of Titan during its accretionary heating phase, when water was presumably in contact with the rocky core (Atreya et al. 2006; 2009). In this scenario, H_2 liberated in serpentinization reacts with primordial carbon in the form of CO, CO_2, or carbon grains in a metal-catalyzed Fischer–Tropsch process to produce methane. Mousis et al. (2009a) surmised that if water-rock reactions were responsible for Titan's methane, the D/H ratio in Titan's CH_4 ($\sim 1.3\times10^{-4}$) should then reflect the value in Titan's water ice. As no measurements are available for D/H in Titan's water ice, they assumed that the D/H ratio measured in the water vapor plumes of Enceladus could serve as a proxy for the D/H in Titan's water. The Enceladus D/H value is 3×10^{-4}, which is more than twice the value in Titan's CH_4. This discrepancy led Mousis et al. (2009a) to propose that Titan's methane was trapped in its building blocks, which agglomerated from icy grains condensed in the protosolar nebula. In this scenario, Titan's methane would originate from ISM and its inferred D/H value would have resulted from the isotopic exchange with the

nebula's hydrogen that occurred until it condensed and was agglomerated by the building blocks of Titan. This conclusion was supported by the measurements of D/H in water in six Oort cloud comets available at that time, all of which have a value that is nearly identical to that measured in Enceladus' H_2O plumes by the Cassini ion and neutral mass spectrometer, and corresponded to more than two times the value of D/H in Titan's methane. However, later observations of Jupiter family comet Hartley 2 yield a D/H ratio of 1.56×10^{-4} in water (Hartogh et al. 2011), which is similar to the value in Titan's CH_4 within the range of uncertainty for both objects. Another Jupiter family comet, 67P/Churyumov–Gerasimenko, on the other hand, yields D/H=5.3×10^{-4} in water (Altwegg et al. 2015), four times higher than in Titan's CH_4. Neither of these two comets has a D/H ratio in water similar to that assumed for Titan's water ice, the Enceladus value. Though the argument of methane trapping from the protosolar nebula appears to be weakened in view of these findings, it remains a plausible mechanism that needs to be validated by future observations, including, for example, direct D/H measurement in Titan's water, D/H in a large number of comets, as well as laboratory studies and modeling.

Two main models have been proposed for the formation of large satellites of the gas giant planets, including Titan. In the first model, the satellite formation takes place in a dense and hot disk at the early stages of the gas giant planet formation (Prinn and Fegley 1981, 1989; Lunine et al. 1989), while the other model uses a thin and cold disk to depict satellite formation (Canup and Ward 2002). In the former model, the chemical composition of Titan's proto-atmosphere would have been primarily CH_4 and NH_3. These gases would have been produced, prior to planetesimal condensation, from CO and N_2 initially present in the dense, hot, and chemically active CPD (Prinn and Fegley 1989; Sekine et al. 2005). This scenario may be ruled out for the bulk of Titan's nitrogen on the basis of the nitrogen isotope ratio, with the caveat about atmospheric escape, as discussed below. In Titan's atmosphere, $^{14}N/^{15}N = 167.7$ (Niemann et al. 2010), which is much less than, not similar to, the value in Saturn (>357; Table 2.3, Section 2.2.1), which implies that the ammonia accreted by Titan did not originate from the protosolar nebula. On the other hand, the present nitrogen isotope ratio depends on the evolutionary history and the processes of escape of nitrogen from Titan early on and in the past 4.5 Gyr, which are very poorly constrained. Even on Earth and Venus, which have atmospheres as dense as or even denser than Titan, escape processes have shaped their present atmospheric isotope ratios. Additional modeling and observations are needed to resolve the issue of evolution of Titan's nitrogen isotope ratio over time.

The other model suggests that icy planetesimals were actively supplied into the CPD from Saturn's feeding zone in the solar nebula (Canup and Ward 2002; Alibert and Mousis 2007). In this scenario, the chemical composition of Titan's proto-atmosphere would derive from that of CO- and N_2-rich icy planetesimals formed at low temperature (~20 K) in the protosolar nebula (see Section 2.4.1 for details concerning the composition of the protosolar nebula). However, similar to the previous case, this scenario is found to be inconsistent with the low $^{14}N/^{15}N$ ratio measured in Titan's nitrogen, but with the caveat of nitrogen escape mentioned above. In order to solve these discrepancies, Mousis et al. (2009b) proposed that Titan was formed from icy planetesimals initially produced in the solar nebula that were partially devolatilized during their migration within Saturn's CPD. By doing so, Titan's building blocks preserved the ammonia and methane they acquired from the protosolar nebula and released most of the carbon monoxide and nitrogen prior to satellite formation. However, as discussed above, production of methane on Titan by serpentinization, rather than direct delivery of CH_4, is also an attractive possibility.

Considering the lack of full complement of relevant observational constraints for Titan, Saturn, and the comets, clear discrimination between the two scenarios is not possible at this time. It is also plausible that both mechanisms could have played a role to varying degrees. Nevertheless, above considerations about Titan's composition still allow us to place important constraints on the thermodynamic state of Saturn's CPD at the time of formation of its largest satellites. In view of the low $^{14}N/^{15}N$ ratio measured in Titan's atmosphere, it seems that the CPD may not have been warm and dense enough to allow in situ condensation of its building blocks, but available observational constraints are insufficient to make a firm statement, as discussed above. On the

other hand, a temperature-density gradient probably did exist throughout Saturn's CPD, not important enough to allow the vaporization of water ice at Titan's formation zone, but probably sufficient to explain why Titan's primordial nitrogen reservoir is NH_3 and not N_2, as is the case for Saturn (Mandt et al. 2014).

The above two models focus on the dominant body only (Titan) and somehow disregard the system of regular satellites of Saturn as a whole. However, a recent scenario for the formation of the regular satellites interior to Titan provides constraints on Saturn's history and internal structure. The rings spread, and spread faster when they are more massive, so that after about 4 Gyr of evolution, they should have roughly the present mass, whatever their initial mass (Salmon et al. 2010). Hence, it is possible that they originally were thousands of times more massive than now (e.g. Canup 2010). As the rings spread beyond the Roche radius, they agglomerate into moonlets, which migrate outwards due to their interaction with the rings (Charnoz et al. 2010). Numerical simulations show that this process can generate the 10 regular satellites inside Titan, and even explain the irregular silicate cores of the 5 largest ones (Charnoz et al. 2011). Crida and Charnoz (2012) solved analytically the equations governing the formation and migration of satellites from the spreading of rings beyond the Roche limit and found that the mass-distance relation in a system of satellites formed in this manner must follow a particular power law, which is represented in Figure 2.6. The agreement with the observed distribution supports this model. Even Titan lies on the theoretical line, which could be a coincidence, or not. Iapetus doesn't fit in this model and is not shown in the figure (it would be further on the middle right), but Iapetus is thought to have formed concurrently with Saturn in the circumplanetary disk (Castillo-Rogez et al. 2009).

It is possible that the regular satellites inside Titan formed after Titan and Saturn, from the spreading of initially massive rings. But for this to happen within the age of the solar system, strong tidal dissipation is needed inside Saturn. Tidal dissipation is characterized by a dimensionless factor, generally denoted as Q; the lower the value of Q, the stronger the dissipation. Charnoz et al. (2011) found that with Q on the order of 1700, as argued by Lainey et al. (2012, 2015), the formation of Saturn's satellite system takes about 3.5

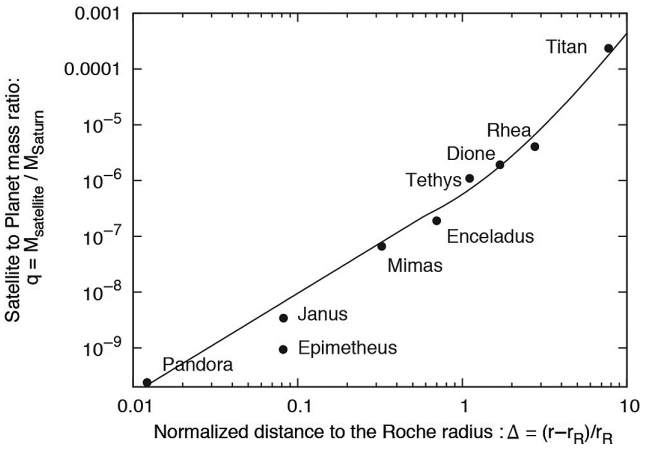

Figure 2.6 Satellite-to-planet mass ratio q as a function of the normalized distance to the Roche radius, located at the outer edge of the rings, 140,000 km away from Saturn's center. The line corresponds to the model described in Section 2.3.4. Adapted from Figure 1 of Crida and Charnoz (2012). Reprinted with permission from AAAS.

Gyr (present satellite crater density record does not provide unambiguous evidence either in favor of or against this timescale). The standard value of Saturn's Q used to be an order of magnitude larger (corresponding to ten times less dissipation), but one should consider that this high value was supported by the constraint that the satellites were supposed to have hardly moved since the formation of the solar system, which may be incorrect. In contrast, the Lainey et al. value is based on observations and is consistent with this new model for satellite formation. In the end, models of the formation of the satellites allow us to place constraints on the efficiency of the dissipation inside Saturn, and hence on its interior. Remus et al. (2012) show that low values of Q (high dissipation rates) are possible in the framework of a model in which tidal dissipation occurs at the interface between the core and the envelope as a result of different anelastic deformations. Values as low as 10^3 require a specific range of values of the shear modulus and viscous modulus in the core. Unfortunately, these two quantities are almost unknown, given the uncertainties on the size, composition, and physical state of the core.

2.4 Saturn's Formation: Chemical Point of View

Just as the hydrodynamical scenario discussed in the previous section provides insight into Saturn's origin,

chemical evolution of the protosolar disk and the manner in which volatiles are sequestered in grains or planetesimals, together with their nature and delivery to Saturn, provide valuable constraints to the models of Saturn's formation and evolution. This section elaborates on these processes.

2.4.1 Chemical Evolution of the Protosolar Disk

Formation scenarios of the protosolar nebula invoke two reservoirs of ices, namely an inner and an outer reservoir, which took part in the production of icy planetesimals. The first reservoir contains ices (mostly water ice) originating from the ISM, which were initially vaporized due to their proximity to the Sun. With time, the decrease of temperature and pressure conditions allowed the water in this reservoir to condense at ~150 K in the form of microscopic crystalline ice on the surface of pre-existing refractory grains (Kouchi et al. 1994). The other reservoir, located at larger heliocentric distances, is composed of ices originating from the ISM that were preserved when entering into the disk. In this reservoir, water ice was essentially in the amorphous form and the other volatiles remained trapped in the amorphous matrix (Notesco and Bar-Nun 2005). The exact localization of the boundary between these two reservoirs, corresponding to the initial location of the so-called "iceline," depends on the assumed thermal structure of the disk, which is still poorly constrained. Optically thin disks such as the steady nebula model of Hayashi (1981) predict that the water iceline is located just beyond the Main Belt (also known as the Asteroid Belt, which is located between the orbits of Mars and Jupiter, or 2.2–3.2 AU). On the other hand, optically thick models of the protosolar nebula suggest that the water iceline might have been initially up to ~30 AU from the Sun (Chick and Cassen 1997).

The O-, C-, and N-bearing ices delivered from ISM to the protosolar nebula are expected to be essentially constituted from H_2O, CO, CO_2, CH_3OH, CH_4, N_2 and NH_3, with H_2O, CO, CO_2 and N_2 being the most abundant molecules in decreasing order (Öberg et al. 2011a; Gibb et al. 2004). H_2O ice is expected to be dominant because (i) of its high abundance (due to the cosmic abundance of H and O) and (ii) it is by far the first volatile to condense as the temperature decreases in the nebula.

Regardless of the considered volatile reservoir in the protosolar nebula, dust and ice particles coagulated until they reached cm-sized pebbles. Once formed, these pebbles agglomerated into large planetesimals (10–1000 km) by streaming instabilities (Youdin and Goodman 2005; Johansen and Youdin 2007; Johansen et al. 2009) and formed the cores of the giants on timescales that were sufficiently short to allow in situ formation of these planets prior to their migration in the protosolar nebula (Lambrechts et al. 2014). Pebbles and planetesimals formed in the outer reservoir should have coagulated from pristine amorphous ice originating from ISM. In contrast, pebbles and planetesimals formed during the cooling of the inner reservoir coagulated from a mixture of microscopic icy grains made of pure condensates, stoichiometric hydrates (such as NH_3-H_2O) and clathrates, whose proportions depended on the availability of water ice and the temperature to which the disk had cooled down.

2.4.2 Delivery of Volatiles to Saturn via the Accretion of Planetesimals

Several hypotheses relating the thermodynamic evolution of the protosolar nebula to the formation conditions of the giant planets have been developed in order to interpret their observed volatile enrichments. In particular, the volatile enrichments observed in the giant planets can be explained by the accretion of icy planetesimals and their vaporization in the envelopes at the time of their growth from nebular gas. The two main scenarios proposed in the literature, each based on the hypothesis that the giant planets accreted planetesimals originating from one of the two abovementioned reservoirs of ices, are discussed below.

Delivery of Amorphous Ices to Saturn

Owen et al. (1999) proposed a cold icy planetesimal model, according to which the volatile enrichments observed by the Galileo probe in Jupiter result from the accretion of planetesimals agglomerated from amorphous ice at temperatures below approximately 30 K (such low temperatures are needed to trap N_2 and Ar; Owen et al. 1999). Owen et al. postulated that either Jupiter was formed at large heliocentric distances of 40–50 AU, where the cold temperature favored the

preservation of amorphous ice in the disk, and then migrated to its current location, or the protosolar nebula was much cooler at the current location of Jupiter (~5 AU) than what is predicted by current turbulent accretion disk models. In either case, the icy material originated from the protosolar cloud and survived the formation of the protosolar nebula. If correct, this scenario predicts that the volatile enrichments should be uniform (also, Owen and Encrenaz 2006), since volatiles are not fractionated when trapped in amorphous ice. However, as discussed in Section 2.2.1, current analysis of the Galileo Probe data shows that the enrichment of the observed heavy elements spans a range of 2 to 6 times the current solar elemental abundances. For Saturn, key data needed to assess the validity of the icy planetesimal model or another model are presently lacking. Noble gases are not measured. Amongst non-noble gases, the only heavy element with a robust value is carbon, with C/H approximately 9× solar (Table 2.1). Sulfur enrichment is similar to carbon, but the result is tentative (Section 2.2.1). NH_3 is a good measurement, but currently provides N/H only in the 1- to 3-bar region. As discussed earlier (Section 2.2.1), it is far from certain that the N/H value in the deep well-mixed atmosphere of Saturn is going to be similar; it could be greater. If one assumes that the N/H in Saturn's deep atmosphere is unchanged from the value at 3 bars, then the C-enrichment is greater than N-enrichment by a factor of 3, not the same, which would argue against the cold icy planetesimal model as presented in Owen et al. (1999). On the other hand, C/S would favor it if the H_2S result were confirmed by future observations.

Delivery of Crystalline Ices to Saturn

An alternative interpretation of the volatile enrichments measured in Jupiter is based on the hypothesis that most of the volatiles were trapped in clathrates in the giant planet's feeding zone (Gautier et al. 2001; Alibert et al. 2005a, 2005b). These authors assumed that Jupiter's building blocks formed in the inner zone of the protosolar nebula, in which the gas phase has been enriched at early epochs by the vaporization of amorphous ice entering from the Interstellar Medium (ISM). During the cooling of this region of the disk, water vapor crystallized and trapped the volatiles in the form of clathrates or stoichiometric hydrates in the 40–90 K range instead of condensing at lower temperatures. These ices then agglomerated and formed the solids that were ultimately accreted in the envelope of the growing Jupiter. These scenarios, which assume the full (100%) clathration of volatiles, are based on the hypothesis that the amount of available crystalline water ice was large enough ($H_2O/H_2 > 2\times(O/H)_{protosolar}$) to trap the other volatiles in the feeding zone of Jupiter. Later studies have shown that it is also possible to explain the volatile enrichments in Jupiter in terms of the accretion and the vaporization in its envelope of icy planetesimals made from a mixture of clathrates and pure condensates (Mousis et al. 2009c, 2012), assuming a full protosolar composition for the gas phase of the disk and provided that the disk's temperature decreased down to ~20 K at their formation location. Figure 2.7 represents a clathration/condensation sequence of volatiles that has been used by Mousis et al. (2012) to interpret the volatile enrichments in Jupiter.

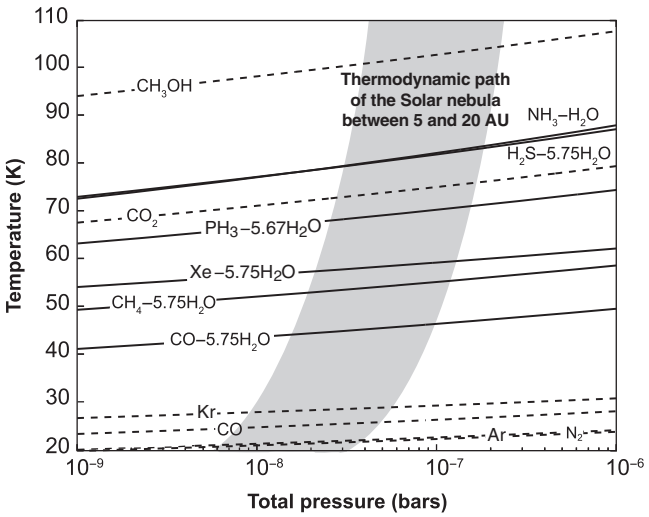

Figure 2.7 Formation conditions of icy planetesimals in the solar nebula. Equilibrium curves of hydrate (NH_3–H_2O; solid line), clathrates (X-5.75H_2O or X-5.67H_2O; solid lines), and pure condensates (dashed lines) are superimposed with the thermodynamic path of the solar nebula in the 5–20 AU range, assuming full clathration efficiency. Elemental abundances are solar, with molecular ratios specified in Mousis et al. (2012). Species remain in the gas phase above the equilibrium curves. Below, they are trapped as clathrates or simply condense. The clathration process stops when no more crystalline water ice is available to trap the volatile species.

In the case of Saturn, if only C enrichment is considered (Section 2.2.1), it is easily explained via the delivery of planetesimals formed at low temperatures, similarly to those accreted by Jupiter. When considering both C and N enrichments measured in Saturn with C/N=3, provided that N/H in the bulk atmosphere is the same as in 1- to 3-bar region, which is far from certain (Section 2.2.1), the scenario of full volatile clathration may not hold anymore because it would result in a uniform enrichment of these two species (Mousis et al. 2006). It has thus been argued that Saturn might have formed at a higher temperature than those required for the formation of CO and N_2 clathrates in the protosolar nebula (Hersant et al. 2008). However, this scenario does not match the high $^{14}N/^{15}N$ ratio recently estimated for Saturn (>357, Table 2.3; Section 2.2.2), since it predicts a value intermediate between the values for Jupiter (434) and the Earth (272). As discussed above, much of the critical heavy element abundance data for Saturn needed to fully evaluate the validity of the clathrate model are missing, and to some extent they are also missing for Jupiter. With 100% efficiency of clathration, models predict approximately 15× solar O/H at Jupiter (e.g. Gautier et al. 2001, using current solar O/H of Asplund et al. 2009), whereas the icy planetesimal model predicts it to be four times less (Owen et al. 1999). Water is critical for discriminating between various formation scenarios. Little laboratory data are presently available for the relatively low pressure conditions of the solar/protoplanetary nebula. In summary, both the cold icy planetesimal model and the clathrate model have their strengths and weaknesses, and discrimination between them requires new sets of data, particularly for Saturn (see Chapter 14 by Baines et al. for additional details).

2.4.3 Role of Photoevaporation of the Protosolar Disk in Determining Present-Day Composition

The atmospheres of the giant planets result from the accretion of both gaseous and solid material by planetary cores. The clathrate scenario implicitly assumes that all species other than hydrogen and helium were delivered with the solids. However, processes affecting the protosolar disk itself may also play an important role in determining the final atmospheric compositions. A plausible scenario proposed by Guillot and Hueso (2006) to explain the homogeneous enrichment of noble gases in Jupiter is illustrated in Figure 2.8. It is based on the fact that protoplanetary disks can extend to hundreds of AU and that their outer parts are generally very cold (e.g. Dartois et al. 2003). Temperatures of 10–30 K in the outer disks allow the direct condensation of most noble gases onto small grains (e.g. Owen et al. 1999). These grains will grow, settle towards the disk mid-plane and migrate inward (e.g. Adachi et al. 1976; Weidenschilling 1984; Dubrulle et al. 1995). In parallel, the gas disk is being accreted by the central star and photoevaporated both due to direct irradiation from the central star (Gorti et al. 2009) and by ambient FUV irradiation from other stars in the cluster (Adams et al. 2004). This evaporation takes place in the disk atmosphere, a region in which the temperature gradient is strongly negative (Chiang and Goldreich 1997). This would prevent a convective transport of species in the mid-plane regions and therefore, Guillot and Hueso (2006) conjecture, hydrogen and helium would preferentially evaporate. This would lead to a progressive homogeneous enrichment of the disk in condensing species. If formed late, giant planets would incorporate gas that is heavy-element rich, and in particular it would be rich in species such as Ar, Kr, and Xe. This theory explains the enrichment in noble gases in Jupiter's atmosphere measured by the Galileo probe and predicts a similar, homogeneous enrichment in Saturn (i.e. with solar Kr/Ar and Xe/Ar ratios). It cannot make predictions on elements that are delivered into giant planets with the solids and for which the story may be more complicated, as illustrated in the previous section.

2.5 Extrasolar Giant Planets Context

The discovery of numerous extrasolar planets in recent years is now allowing us to place the solar system planets in a cosmic context. Over 3600 confirmed exoplanets are known as of July 2017, of which over 500 are giant planets larger (in mass and/or size) than Saturn.[1] The majority of these planets have been detected either through Doppler spectroscopy of their host stars, i.e. the "radial velocity" (RV) method, or by observing transits of the planets in front of their host

[1] Extrasolar Planets Encyclopedia (http://exoplanet.eu) list of currently known exoplanets and their properties

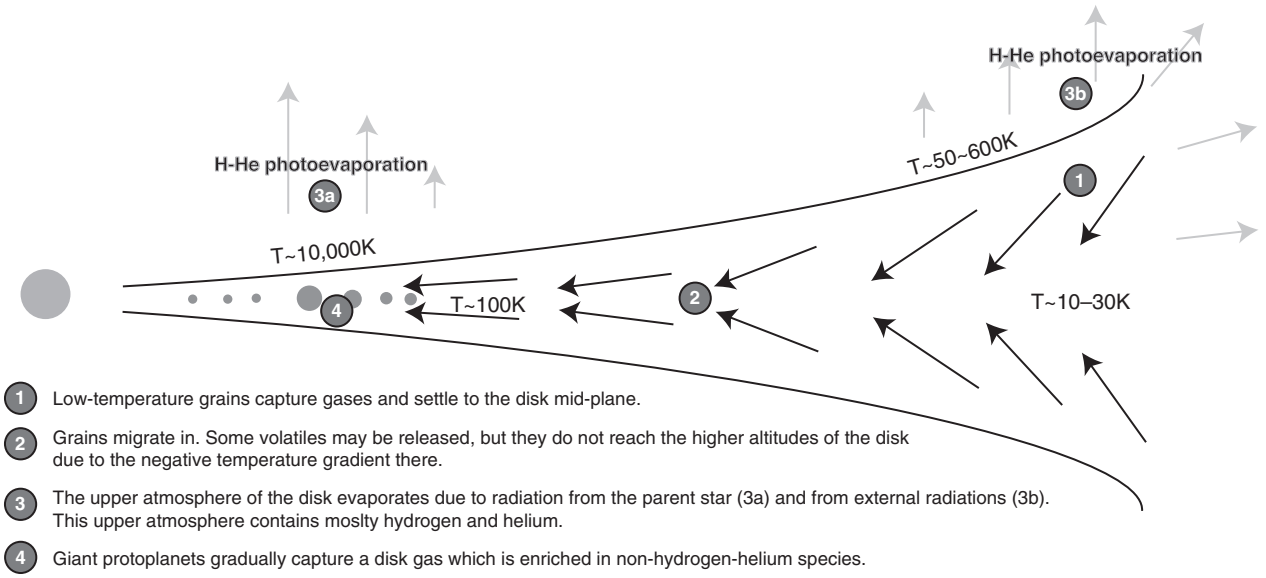

Figure 2.8 Sketch illustrating the scenario proposed by Guillot and Hueso (2006) to explain a homogeneous enrichment of noble gases in the envelopes of giant planets. A gaseous protosolar disk is shown edge-on. Forming protoplanets are shown by grey circles. Black arrows represent the dynamic evolution of grains and noble gases. Yellow arrows correspond to photoevaporation of gas from the disk due to both internal and external UV irradiation. The four circles correspond to the important evolution steps from the condensation of noble gases into cold grains in the outer disk to their incorporation in the envelopes of growing giant planets. (A black-and-white version of this figure appears in some formats. For the color version, please refer to the plate section.)

stars, i.e. the "transit" method, while a few tens of the planets have been detected via direct imaging. The observational sensitivities of the various exoplanet detection methods have precluded conclusive detections of exact analogues of Saturn and Jupiter in exoplanetary systems. Currently, the RV and transit methods, which together allow measurements of the mass and radius of exoplanets, are preferentially sensitive to planets at short orbital separations. Giant exoplanets, with both mass and radius measured, are known at orbital separations of ~0.01 to 0.5 AU, implying equilibrium temperatures over ~1000 K. On the other hand, while the direct imaging method is more sensitive to planets with large orbital separations ($\gtrsim$10 AU), current instruments are only sensitive to young, and hence also hot, giant planets, whose large fluxes make them detectable.

These diverse giant exoplanets form a starting point for placing the properties of solar system giant planets in perspective. In this section, we review our current understanding of the interior, atmosphere, and formation conditions of extrasolar giant planets and their analogies with Saturn and Jupiter in the solar system.

2.5.1 Interiors of Giant Exoplanets

Constraints on the interior composition of giant exoplanets are based primarily on their masses and radii, which are both known for about 200 transiting exoplanets with a mass and radius greater than those of Saturn (0.30 M_J and 0.84 R_J), generally referred to as "hot Jupiters." These planets have revealed an extreme diversity in their bulk parameters, with masses of 0.3 to 20 M_J, radii of 0.84 to 2 R_J, and temperatures of ~1000 to 3000 K. The masses and radii of these planets are consistent with a gaseous interior dominated by H_2 and He, similar to the interior of Saturn and Jupiter in the solar system. However, the diversity in mass and radius also implies a wide range of possible core masses, ranging from no core to ~200 M_E for the heaviest planets (e.g. Guillot et al. 2006; Baraffe et al. 2008), while upper limits on the core mass in Saturn and Jupiter are estimated to be ~10 to 20 M_E, as discussed in Section 2.2.3. Some studies have also suggested a possible positive correlation between the planetary core mass in hot Jupiters and the metallicity of the host star (e.g. Guillot et al. 2006). However, constraints on the core mass in giant exoplanets and on their internal

structure in general are confounded by several complexities (see e.g. review by Baraffe et al. 2014).

Unlike the solar system giants, a large fraction of hot Jupiters have a radius that is significantly larger than would be predicted by internal structure models of giant planets, even assuming no solid core (the presence of a core contracts the planet). The largest planet known, WASP-17b, has a radius of ~2 R_J but a mass of only 0.5 M_J (Triaud et al. 2010). Such bloated giant planets have no analogy in the solar system and cannot be explained by canonical interior models of Saturn and Jupiter. Several mechanisms have been proposed to address the problem that bear on the key factors in which hot Jupiters differ from solar system giant planets. Hot Jupiters receive stellar irradiations that are 3 to 4 orders of magnitude higher than the insolation at Jupiter, and because of their close proximity to their host stars they are also subject to strong tidal and magnetic interactions. The various proposed mechanisms to explain inflated giants, though still actively debated, broadly include (a) deposition of incident energy deep in the planetary atmosphere, causing an extra energy source in the planetary interior and slowing down the thermal evolution, i.e. cooling, of the planet (Guillot and Showman 2002; Batygin and Stevenson 2010; Youdin and Mitchell 2010); (b) intrinsic heating caused by tidal dissipation in the planetary interior due to an eccentric close-in orbit that is being tidally circularized (e.g. Bodenheimer et al. 2001; Leconte et al. 2010); and (c) strong atmospheric opacity that inhibits the emergent flux, thereby delaying the cooling, and hence contraction, of the planet during its evolution (Burrows et al. 2007). However, none of these mechanisms conclusively explains the radius distributions in all the hot Jupiters currently known (see, e.g. Spiegel and Burrows 2013; Baraffe et al. 2014). Consequently, even though hundreds of giant exoplanets are known with similar masses and sizes as solar system giants, their interior structures and compositions are likely extremely diverse, albeit currently underconstrained.

2.5.2 Atmospheres of Giant Exoplanets

Remarkable progress has been made in the past decade in spectroscopic observations of exoplanetary atmospheres, primarily of hot gas giants that are most accessible to current instruments (see, e.g. review by Madhusudhan et al. 2014b). Currently observable gas giant atmospheres fall into two distinct categories: (a) highly irradiated giant planets ("hot Jupiters") in very close orbits (as close as 0.01 AU) and (b) young and self-luminous directly imaged planets at wide orbital separations (beyond ~10 AU). The effective temperatures of either class of planets are in the range of ~1000 to 3000 K, which are an order of magnitude hotter than those of solar system giant planets (~100 to 200 K). Since the radiation field is intricately linked to the physicochemical characteristics of the atmospheres, the atmospheric temperature structure, chemistry and dynamics in these giant exoplanets can be markedly different from those of Saturn and Jupiter in the solar system, even if the masses, radii, and bulk elemental abundances turn out to be similar. Here, we review current understanding of giant exoplanetary atmospheres vis-a-vis our understanding about the atmospheres of Saturn and Jupiter.

Atmospheric Observations

Spectra of exoplanetary atmospheres are inherently disk-integrated, unlike spectra of solar system giant planets, which can be spatially resolved over the planetary disk. Observations of exoplanetary spectra have been obtained using three key methods. Firstly, the atmospheres of close-in hot Jupiters have been observed primarily through transit spectroscopy, obtained during the planet's "transit" in front of the host star or "occultation" behind the star. While a transit (or transmission) spectrum probes the atmosphere of the day-night terminator region of the planet, the occultation (or emission) spectrum probes the dayside atmosphere of the planet. Spectra of transiting hot Jupiters have been observed both from space, using the Hubble and Spitzer space telescopes, as well as from ground-based facilities. While Spitzer and ground-based facilities have typically provided photometric observations of transiting exoplanets in the near-infrared (e.g. Charbonneau et al. 2008; Croll et al. 2011), the Hubble telescope has been instrumental in obtaining spectra across multiple spectral regimes, from the ultraviolet to near-infrared, for a few planets (Vidal-Madjar et al. 2003; Sing et al. 2011; Deming et al. 2013). These state-of-the-art observations have provided both the high precision and a long spectral baseline required to

constrain the atmospheric properties of several transiting hot Jupiters. Secondly, it has also been possible to detect molecules in the atmospheres of a few transiting and non-transiting close-in hot Jupiters using very high resolution (R ~10^5) infrared Doppler spectroscopy using large ground-based telescopes (Snellen et al. 2010). Thirdly, ground-based spectroscopy of directly imaged planets has led to both photometry and high-resolution spectra of thermal emission from several young self-luminous planets in the near infrared (e.g. Marois et al. 2010; Konopacky et al. 2013; Janson et al. 2013).

Atmospheric Chemistry

The chemical compositions of hot giant exoplanets are expected to be markedly different from those of solar system giant planets, even if the bulk elemental abundances may be identical. The bulk molecular composition of the atmospheres of Saturn and Jupiter is generally consistent with expectations for low-temperature (~100 to 200 K) H-rich atmospheres, i.e. those dominated by methane, ammonia and higher-order hydrocarbons (Section 2.2.1). H_2O is expected to be the dominant O carrier but its abundance is presently undetermined in both Saturn and Jupiter because of their low temperatures, as discussed in Section 2.2.1. On the other hand, H_2O is more observable in the high-temperature atmospheres of giant exoplanets. However, the expected molecular composition depends strongly not only on the atmospheric temperatures but also on the elemental abundance ratios, particularly the overall metallicity and the C/O ratio (Madhusudhan 2012; Moses et al. 2013). Assuming solar abundances (i.e. C/O = 0.5), in the 1000 to 3000 K temperature range of hot giant exoplanets H_2O is expected to be the dominant carrier of O in the observable atmosphere and CO is expected to be the dominant C carrier above ~1300 K, while at lower temperatures CH_4 and NH_3 are expected to be abundant, along with trace quantities of CO_2 (Lodders and Fegley 2002; Madhusudhan 2012). Other species expected in hot Jupiters include Na, K, TiO, and VO (Seager et al. 2000; Hubeny et al. 2003; Madhusudhan 2012), which are not found in solar system gas giants because of their low temperatures. The chemistry can be even more drastic for super-solar abundance ratios, e.g. C/O = 1, in which case H_2O can be substantially underabundant and carbon-rich species overabundant, even in very high-temperature atmospheres (Madhusudhan 2012; Moses et al. 2013). Therefore, molecular abundances in hot Jupiters serve as key indicators of their elemental abundance ratios, such as the C/O ratio.

Chemical species have been detected in several giant exoplanetary atmospheres using all three observational methods discussed above. Recently, H_2O has been detected at high statistical significance in the atmospheres of several transiting hot Jupiters using the HST WFC3 spectrograph in the near-infrared (1.1–1.7 μm), e.g. in HD 209458b, HD 189733b, WASP-43b, and WASP-17b (Deming et al. 2013; Mandell et al. 2013; Kreidberg et al. 2014; McCullough et al. 2014). Additionally, transmission spectroscopy in the visible has been used to detect several atomic species in hot Jupiter atmospheres, e.g. Na and K (Redfield et al. 2008; Sing et al. 2011).

More recently, CO and H_2O have been detected in some transiting as well as non-transiting hot Jupiters using ground-based high-resolution infrared Doppler spectroscopy (e.g. Brogi et al. 2012; Birkby et al. 2013). On the other hand, H_2O, CO, and CH_4 have also been detected robustly in the atmospheres of directly imaged young giant exoplanets using high-resolution ground-based spectroscopy (e.g. Janson et al. 2013; Konopacky et al. 2013). The recent detection of a methane-rich giant exoplanet 51 Eri b, roughly twice the mass of Jupiter (Macintosh et al. 2015), represents the closest, albeit young (~20 Myr), analogue to solar-system giant planets. 51 Eri b orbits a Sun-like star, 51 Eridiani, at a Saturn-like orbital separation (13 AU), and like Saturn and Jupiter contains CH_4 as the dominant C-bearing molecule in its atmosphere.

In addition to molecular detections, recent observations are beginning to place notable statistical constraints on the molecular abundances in giant exoplanetary atmospheres, suggesting likely diverse elemental compositions. On one hand, some of the highest-precision HST WFC3 near-infrared spectra of transiting hot Jupiters are revealing significantly weaker H_2O features than expected for solar-composition atmospheres. For example, the thermal emission spectrum of the hot Jupiter WASP-12b suggest 100× sub-solar H_2O and a C/O ≥1, in its dayside atmosphere (Madhusudhan 2012; Stevenson et al. 2014), and that

of WASP-33b suggests ~5 to 10× sub-solar H_2O, but with C/O < 1 (Haynes et al. 2015). Similarly, high-precision transmission spectra of the day-night terminator regions of hot Jupiters HD 189733b and HD 209458b suggest H_2O abundances as low as 100× sub-solar, assuming cloud-free models (Deming et al. 2013; Madhusudhan et al. 2014b). It is possible that the presence of high-temperature silicate clouds/hazes as discussed below could be masking the spectral features in some transmission spectra. On the other hand, thermal emission and transmission spectra of the hot Jupiter WASP-43b (semimajor axis 0.01526 AU, orbital period 0.81 days, planetary mass 2 M_J, host star mass 0.717 $M_\odot$ and $T_\odot$ 4520 K) reveal H_2O abundances in the range of 0.4 to 3.5× solar at 1σ confidence level and an upper limit of 20× solar at 3σ confidence level (Kreidberg et al. 2014). Thus, there is a real possibility of super-solar O/H in at least some extrasolar giant planets. Only when H_2O is measured in well-mixed atmospheres of Saturn and Jupiter, direct comparison with O/H in exoplanets will be possible. Meanwhile, consistency between the super-solar O/H in WASP-43b and super-solar C/H in all solar-system giant planets and super-solar Ar, Kr, Xe, N, and S in Jupiter seems to indicate similar formation processes of at least some hot Jupiters and Jupiter and Saturn in the solar system, but much further work is needed to be confident.

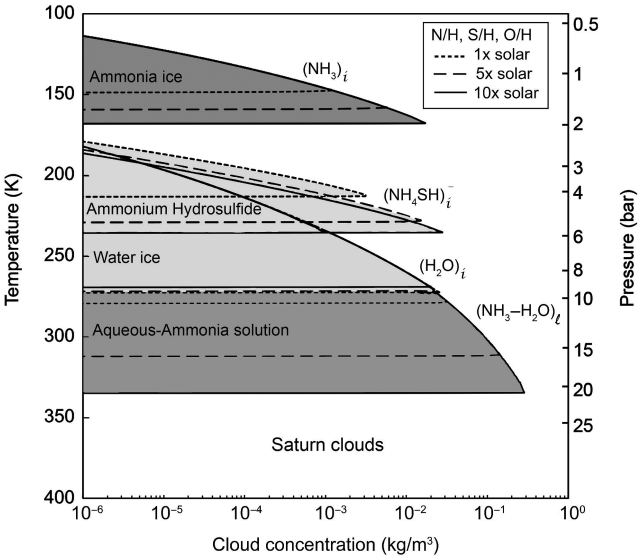

Figure 2.9 Equilibrium cloud condensation model of Saturn, assuming uniform enrichment of 1× solar, 5× solar, and 10× solar abundances for each of the condensible volatiles, NH_3, H_2S, and H_2O, and hence the elemental ratios N/H, S/H, and O/H, respectively. Calculations are based on current solar elemental abundances (Asplund et al., 2009) from Table 2.1. (Note that H_2S does not directly condense, but NH_4SH produced by the vapor-phase reaction between H_2S and NH_3 does in solid form [$(NH_4SH)_i$].) Water can condense as ice $(H_2O)_i$, and liquid of water-ammonia solution ($(NH_3$-$H_2O)_l$, colloquially, windex cloud) for large enrichment of H_2O. The cloud concentrations represent *upper limits*. Precipitation and dynamics would almost certainly deplete cloud densities by up to several orders of magnitude, as in the water clouds in the Earth's troposphere. The cloud bases (or, lifting condensation levels) are robust, however. More realistic cloud densities are formulated in Wong et al. (2015). Figure format adapted from Figure 23.2 in "Saturn Exploration Beyond Cassini–Huygens," by T. Guillot, S. K. Atreya, S. Charnoz, M. Dougherty, P. Read, in Saturn from Cassini–Huygens (M. K. Dougherty et al., eds.), Chapter 23, pp. 745–761, 2009, with permission from the publisher. The present figure is based on entirely new calculations, however. (A black-and-white version of this figure appears in some formats. For the color version, please refer to the plate section.)

Clouds and Hazes

Clouds are ubiquitous in Saturn and Jupiter, but with quite different chemical compositions (Sections 2.2.1 and 2.6) from those expected in giant exoplanets. While clouds in Saturn and Jupiter are presumably made of low-temperature (150 to 300 K) condensates of ammonia, hydrogen sulfide (combined with ammonia), and water, as discussed in Section 2.2.1 and illustrated in Figure 2.9, those in hot giant exoplanets (at 1000 to 3000 K) are expected to be composed of refractory compounds such as silicates, alkali chlorides, Fe, etc. (Sudarsky et al. 2003). To date there is no spectral signature of a cloud-forming condensate in an exoplanetary atmosphere. Instead, the inferences of clouds in these atmospheres are derived from non-detections of expected atomic or molecular features (i.e. due to possible obscuration from clouds) or from modulations in the planetary spectrum indicative of particulate scattering (e.g. a steeper slope rising blue-ward than would be expected from pure gaseous Rayleigh scattering). For example, non-detections of strong Na and K absorption in the visible wavelengths (at 589 nm and 770 nm, respectively) along with a steep power-law spectrum have been suggested as indicative of haze in the hot Jupiter HD 189733b (Sing et al. 2011; Pont et al. 2013). The presence of clouds has also been inferred from observations of visible reflected light and phase

curves of hot Jupiters (Demory et al. 2013; Evans et al. 2013; Barstow et al. 2014). On the other hand, several studies have used near-infrared observations of thermal emission from directly imaged giant planets, such as HR 8799b,c,d,e to suggest the presence of thick clouds in their atmospheres (e.g. Marois et al. 2010; Currie et al. 2011; Marley et al. 2012). Although hazes and clouds are not expected to be made up of H_2O in hot Jupiters due to their atmospheric temperatures that are high enough to vaporize water, they could still remove O from gas phase in the form of condensed silicates, thereby decreasing the amount of O available for H_2O. They could also provide adsorption/sequestration sites for water vapor (and other volatiles) that may result in the removal of H_2O by heterogeneous chemistry or surface processes, depending on the nature of hazes and temperatures.

Temperature Profiles and Stratospheres

Accurate determination of the atmospheric temperature profiles is important to constrain various thermal processes in exoplanetary atmospheres, and also because the temperature gradient is degenerate with chemical composition in their contributions to an emission spectrum (Madhusudhan and Seager 2010). One of the long-standing conundrums in the field concerns the possibility of temperature inversions (or "stratospheres") in exoplanetary atmospheres, i.e. temperatures increasing with altitude in the atmosphere, as opposed to a monotonically decreasing temperature profile, which would be expected for an isolated body. The Earth and larger planets in the solar system all have thermal inversions; on Earth it is due to ozone, in giant planets it is due to hydrocarbon haze. Early theoretical studies (Hubeny et al. 2003; Fortney et al. 2008) predicted that atmospheres of hot Jupiters could also host thermal inversions, but due to very different sources than those in Jupiter or Saturn, namely from gaseous TiO and VO, which can survive at high temperatures. Current observations suggest that some hot Jupiters show "tentative" evidence for thermal inversions whereas others do not (e.g. Stevenson et al. 2014; Haynes et al. 2015). Various processes have been proposed to explain possible trends, e.g. correlations with stellar irradiation (Fortney et al. 2008), TiO condensation (Spiegel et al. 2009), stellar activity (Knutson et al. 2010), C/O ratios (Madhusudhan 2012), and thermoresistive instability (Menou 2012).

Overall, there are presently no conclusive constraints on the presence of thermal inversions in exoplanetary atmospheres or on any inversion-causing absorbers. High-resolution spectra from future facilities would be required to make robust detections of thermal inversions. Although detailed data on thermal structure of the atmospheres of Saturn and Jupiter exists as a result of spacecraft remote sensing and entry probe (at Jupiter) measurements, thermal structure of cold gas planets is not a suitable guide for what to expect in hot Jupiters whose structure is controlled by extreme stellar forcing. However, with appropriate modifications, radiative transfer models used for interpreting temperature observations of cold, clear, cloudy, or hazy gas planets are to some degree applicable to hot Jupiters (Lee et al. 2012).

2.5.3 Formation of Giant Exoplanets

The large population of giant exoplanets provides a diverse sample to test theories of formation of giant planets in the solar system. As discussed in Section 2.1, two main formation mechanisms have been proposed to explain the formation of Saturn and Jupiter: core accretion (CA) and gravitational instability (GI), with clear preference for CA. Various efforts have been made to identify if either of these formation mechanisms could explain the formation of giant exoplanets based on their observed orbital parameters and chemical compositions.

Dynamical Constraints

The diverse orbital parameters of different classes of giant exoplanets (close-in versus distant) constrain the different possible formation mechanisms. In the CA model (Pollack et al. 1996), the planetary embryos start out as ~10 M_E cores in the protoplanetary disk that subsequently undergo runaway accretion of a large volume of gas and planetesimals to form a massive gaseous envelope. On the other hand, a GI in a young disk can cause rapid collapse of a large volume of ambient gas and solids to form a giant planet (Boss et al. 2000). Both scenarios occur in planet-forming disks,

but at different orbital separations. While CA is favored closer to the snowline (within ~2 to 10 AU) because cores take too long to form at larger distances and only reach large masses after the disk has dispersed, GI is favored at larger distances ($\gtrsim$10 AU) where the disk can cool sufficiently on orbital timescales to fragment. In this regard, GI may be the favored mechanism for the formation of distant gas giant exoplanets detected via direct imaging. However, neither GI nor CA is thought to operate in such a way that allows hot Jupiters to form in situ at their current locations close to the host stars. The disk cannot fragment at those distances, and cores with sufficient mass to attract significant envelopes cannot form. Therefore, the existence of hot Jupiters requires some form of "migration" from their original formation locations to their present orbits (see Section 2.3.2).

Migration may occur relatively early in the planet's history via the planet's interaction with, and transport through, the protoplanetary disk while the gas in the disk is still present (Lin et al. 1996). Alternately, migration may also occur at any time via scattering (Rasio and Ford 1996) or secular interactions, such as Kozai resonances (Fabrycky and Tremaine 2007), of the planet with other massive planetary or stellar components in the system. Measurements of orbital obliquities, i.e. the degree of alignment between the stellar equatorial plane and the planetary orbital plane, have been proposed to distinguish between the two migration scenarios (Gaudi and Winn 2007). Whereas migration of a planet through a viscous disk would be expected to damp any initial misalignment, migration by scattering or Kozai resonances could lead to very high spin-orbit misalignments. The observations of a significant number of large spin-orbit misalignments in hot Jupiter systems in recent years initially supported the role of migration by scattering phenomena (Winn et al. 2010; Triaud et al. 2010). However, more recent studies have shown that spin-orbit misalignments can also be caused by planet migration through disks, which are themselves misaligned due to torques induced by a distant stellar companion (Crida and Batygin 2014). Consequently, dynamical measurements alone have not been able to conclusively constrain the formation of hot Jupiters, though directly imaged planets at wide separations ($\gtrsim$10 AU) seem more likely to be formed via GI.

Chemical Constraints

Atmospheric elemental abundances of solar-system giant planets have led to important constraints on the origins of the solar system. For example, the observed super-solar enrichments of C, S, N and the heavy noble gases (Section 2.2.1) support the formation of Jupiter and Saturn by core-accretion (see Sections 2.1 and 2.2.1). However, the oxygen abundance, which is a critical parameter in formation models, is not known in Saturn and Jupiter (see Sections 2.2.1 and 2.6). On the other hand, as discussed in Section 2.5.2, given the high temperatures of currently known giant exoplanets (T ~1000 to 3000 K), several key molecules are expected to be observable in their atmospheres and allow estimations of elemental abundance ratios involving H, C, O, and N. Nominal constraints on atmospheric C/H, O/H, and C/O ratios have already been reported for a few exoplanets and reveal both oxygen-rich (C/O < 1) as well as carbon-rich (C/O $\geq$ 1) compositions; the solar composition is oxygen-rich with C/O = 0.5.

Findings of super-solar C/O ratios in giant exoplanets are beginning to motivate new ideas on their formation mechanisms. The C/O ratios of most planet-hosting stars in the solar neighborhood are solar-like, i.e. oxygen-rich (e.g. Delgado-Mena et al. 2010). Thus, in the standard core-accretion model of planet formation, it is expected that oxygen-rich planetesimals with abundant H_2O ice would dominate the planetesimal composition. Thus, the possibility of C-rich giant planet atmospheres orbiting O-rich stars poses a challenge to standard formation models of Jupiter and Saturn. An early investigation into this question was pursued in the context of Jupiter in the solar system for which, as discussed above, only a lower limit on the O/H is known, which may allow for the possibility of C/O > 1. Lodders (2004) suggested the possibility of Jupiter forming by accreting tar-dominated planetesimals instead of those dominant in water ice, as expected in the solar system based on the composition of minor bodies in the solar system. Following the inference of C/O $\geq$ 1 in the hot Jupiter WASP-12b (Madhusudhan et al. 2011a), Öberg et al. (2011b) suggested that C/O ratios in giant exoplanetary envelopes depend on the formation location of the planets in the disk relative to the

icelines of major C- and O-bearing volatile species, such as H_2O, CO, and CO_2. The C/O ratio of the gas in the nebula approaches 1 outside the CO and CO_2 icelines. By predominantly accreting such C-rich gas, more so than O-rich planetesimals, gas giants could host C-rich atmospheres even when orbiting O-rich stars. It may also be possible that inherent inhomogeneities in the C/O ratios of the disk itself may contribute to higher C/O ratios of the planets relative to the host stars (Madhusudhan et al. 2011b). Additionally, the composition of the planet is also influenced by the temporal evolution of the chemical and thermodynamic properties of the disk at the formation location of the planet Saturn (Ali-Dib et al. 2014; Helling et al. 2014; Marboeuf et al. 2014). More recently, Madhusudhan et al. (2014c) suggested that O and C abundances of hot Jupiters could also provide constraints on their migration mechanisms. In particular, hot Jupiters with sub-solar elemental abundances are more likely to have migrated to their close-in orbits by disk-free mechanisms (e.g. scattering) rather than through the disk, regardless of their formation by core accretion or gravitational instability process.

Thus, various scenarios of giant planet formation and migration predict different limits on the metallicites and C/O ratios of giant exoplanets, which are testable with future high-precision and high-resolution observations of their atmospheres as will be possible with facilities like the *James Webb Space Telescope*, large ground-based telescopes of the future and dedicated space missions. As tighter constraints on the elemental abundances in exoplanets become available, investigating them together with elemental abundances in Saturn and Jupiter will allow development of convincing scenarios of the formation of gas giant planets in the solar system and extrasolar systems.

2.6 Outstanding Issues and Looking to the Future

Existing observations of Saturn, its atmosphere, rings and the moons have provided tantalizing clues into the formation and evolution scenarios of the Saturnian system. Additional insight has come from volatile composition and abundance data of giant exoplanets. Yet, the current observational constraints for developing robust models are either inadequate, poor, or simply non-existent, including those needed to address such fundamental questions as "does Saturn have a core today," "how does the size of Saturn's core compare to Jupiter's core," "what's Saturn's true intrinsic rotation rate," "what's Saturn's bulk composition – in particular, the abundance of heavy elements – and how does it compare with Jupiter's bulk composition," "what's the helium abundance in the troposphere of Saturn," "is the history of heavy noble gases different from that of other heavy elements," and "what are the isotope ratios of H, He, N, S, Ar, Ne, Kr and Xe, and what are their implications." New types of observations are required to address these issues. In the near future, the Cassini Grand Finale Mission appears promising for answering some of these questions.

Following a spectacular tour of the Saturnian system since reaching Saturn in 2004, the Cassini orbiter will enter its final phase of the mission in 2016, aptly named the Cassini Grand Finale, before the spacecraft crashes and burns in Saturn's atmosphere mid-2017. In the final 22 proximal orbits, Cassini's trajectory will take it high above the north pole, flying outside the F-ring and then plunging between Saturn and its innermost ring, skimming as close as ~1700 km above Saturn's cloud tops. These proximal orbits will give an unprecedented opportunity to carry out high-precision measurements of higher-order moments of gravity and magnetic fields and the ring mass and particle distribution. These observations will provide useful constraints on the internal structure, rotation rate and the age of Saturn's rings. As the orbits of the Juno spacecraft at Jupiter will be very similar to Cassini proximal orbits, a comparison between Jupiter and Saturn results in terms of the gravitational and magnetic fields will be possible. This extraordinary opportunity to gather comparable data on Jupiter and Saturn will help us not only to understand the intrinsic differences between these bodies but also to get a sense of the variation we might expect among extrasolar giant planets within the same stellar system. The atmospheric composition relevant to Saturn's formation models requires in situ measurements, however.

Bulk composition and the atmospheric isotope determination of the giant planets cannot be carried out by remote sensing, for the most part. The abundances of He and the heavy elements C, N, S, O, Ne, Ar, Kr, and Xe and isotope ratios D/H in H_2, $^3He/^4He$,

$^{13}C/^{12}C$, $^{15}N/^{14}N$, and $^{34}S/^{32}S$ and the isotope ratios of the heavy noble gases are crucial constraints on the formation models. With the exception of carbon, their determination requires an entry probe at Saturn, as was done at Jupiter with the Galileo probe in 1995 (note the remote sensing result on D/H at Saturn is imprecise). A shallow-entry probe to 10 bars at Saturn is expected to deliver meaningful data on all of the above elements and isotopes, except perhaps oxygen, unless O/H is substantially sub-solar in Saturn. This is evident from Figure 2.9, which shows the equilibrium cloud condensation levels of the condensible volatiles in Saturn's troposphere. For solar O/H, the base of the water cloud is found to be at 10 bars (cloud densities in the figure are *upper limits*; cloud bases are robust, however). As discussed earlier, water may be enriched similarly to carbon, i.e. roughly 10× solar. In that case, the base of the water cloud would be at ~20 bars. Because of convective and dynamical processes, well-mixed water may not be reached above two to three times these pressure levels, however. Thus, even in the unlikely scenario of solar water, only probe measurements to at least 20 to 30 bars can ensure reliable O/H determination in Saturn. If water is 10× solar, measurements down to at least 50 bars, preferably 100 bars, will be required for the O/H determination. If water in Saturn is greatly sub-solar, probes to 10 bars will be able to determine the O/H directly in Saturn. Deep probes to such extreme environments of high pressures and temperatures and large radio opacity are presently unfeasible. However, Juno-like microwave radiometry from orbit at Saturn could potentially map the deep water abundance over the planet, thus allowing the determination of the O/H ratio. Although O/H ratio in Saturn is desirable, its absence due to technical hurdles or cost constraints would not be a disaster. Comparison of all other elements and isotopes in Saturn, particularly the noble gases, with those in Jupiter measured by the Galileo probe and Juno's O/H would establish a trend or pattern from one gas giant planet to the other, which may still provide meaningful constraints on Saturn's O/H. Other reservoirs of oxygen, such as CO, though much less abundant than H_2O, could also be exploited to obtain clues to the limits of O/H in Saturn. Future ground-based microwave measurements with improved capability are also promising for the deep water abundance. Refer to Chapter 14 by Baines et al. for additional details on future exploration of Saturn.

Finally, composition data including especially the profiles of H_2O, CO, and CH_4 in the atmospheres of giant exoplanets can provide a useful guide for Saturn. Similarly, in many respects, Saturn and Jupiter are ideal analogs for similar-sized exoplanets around sun-like stars, despite the differences in their current orbital distances and resulting temperatures. Spectroscopic characterization of exoplanet atmospheres is proceeding rapidly, and there is a good prospect of addressing many of the outstanding issues including temperature structure and aerosol distribution. A comparison between atmospheric properties of a multitude of giant exoplanets is also essential. This chapter demonstrates that cross-fertilization between the giant planet research and the giant exoplanet research is beneficial both fields, and leads to a deeper understanding of the origin and evolution of this solar system and the extrasolar systems.

Acknowledgments

Discussions with several colleagues on the Juno, Cassini and Galileo science teams and ground-based planetary astronomers were beneficial in preparing this chapter. Joong Hyun In, Gloria Kim, and Carmen Lee assisted with references and formatting.

References

Adachi, I., C. Hayashi and K. Nakazawa (1976), The gas drag effect on the elliptical motion of a solid body in the primordial solar nebula, *Prog. Theor. Phys*., **56**, 1756–1771.

Adams, F. C., D. Hollenbach, G. Laughlin et al. (2004), Photoevaporation of circumstellar disks due to external far-ultraviolet radiation in stellar aggregates, *Astrophys. J*., **611**, 360–379.

Alibert, Y. and O. Mousis (2007), Formation of Titan in Saturn's subnebula: Constraints from Huygens probe measurements, *Astron. Astrophys*., **465**, 1051–1060.

Alibert, Y., Mousis, O. and Benz, W. (2005a), On the Volatile enrichments and composition of Jupiter, *Astrophys. J*., **622**, L145–L148.

Alibert, Y., O. Mousis, C. Mordasini et al. (2005b), New Jupiter and Saturn formation models meet observations, *Astrophys. J*., **626**, L57–L60.

Ali-Dib, M., O. Mousis, J. M. Petit et al. (2014), Carbon-rich planet formation in a solar composition disk, *Astrophys. J*., **785**, 125–131.

Altwegg, K., H. Balsiger, A. Bar-Nun et al. (2015), 67P/Churyumov-Gerasimenko: A Jupiter family comet with a high D/H ratio, *Science*, **347**(6220). 1261952–1 – 1261952–3.

Amelin, Y. A., A. Kaltenbach, T. Iizuka et al. (2010), U-Pb chronology of the solar system's oldest solids with variable $^{238}U/^{235}U$, *Earth Planet. Sci. Lett*., **300**, 343–350.

Anders, E. and N. Grevesse (1989), Abundances of the elements: meteoritic and solar, *Geochim. Cosmochim. Acta*, **53**, 197–214.

Armitage, P. (2010), *Astrophysics of Planet Formation*, Cambridge University Press, Cambridge.

Arpigny, C., E. Jehin, J. Manfroid et al. (2003), Anomalous nitrogen isotope ratio in comets, *Science*, **301**, 1522–1524.

Asplund, M., N. Grevesse, J. Sauval et al. (2009), The chemical composition of the Sun, *Annu. Rev. Astron. Astrophys*, **47**, 481–522.

Atreya, S. K. (1986), *Atmospheres and Ionospheres of the Outer Planets and their Satellites*, pp. 66–79. Springer-Verlag, New York-Heidelberg.

Atreya, S. K., E. Y. Adams, H. B. Niemann et al. (2006), Titan's methane cycle, *Planet. Space Sci*., **54**, 1177–1187.

Atreya, S. K., T. M. Donahue and W. R. Kuhn (1978), Evolution of a nitrogen atmosphere on Titan, *Science*, **201**, 611–613.

Atreya, S. K., R. D. Lorenz and J. H. Waite (2009), Volatile origin and cycles: Nitrogen and methane, in *Titan from Cassini-Huygens*, edited by R. H. Brown, J. P. Lebreton, and J. Waite, pp. 177–199, Springer Dordrecht, Heidelberg-London-New York.

Atreya, S. K., P. R. Mahaffy, H. B. Niemann et al. (2003), Composition and origin of the atmosphere of Jupiter: An update, and implications for the extrasolar giant planets, *Planet. Space Sci*., **51**, 105–112.

Atreya, S. K., M. G. Trainer, H B. Franz et al. (2013), Primordial argon isotope fractionation in the atmosphere of Mars measured by the SAM instrument on Curiosity, and implications for atmospheric loss, *Geophys. Res. Lett*., **40**, 5605–5609.

Atreya, S. K. and A. S. Wong (2005), Coupled chemistry and clouds of the giant planets: A case for multiprobes, *Space Sci. Rev*., **116**, 121–136.

Atreya, S. K., M. H. Wong, T. C. Owen et al. (1999), A Comparison of the atmospheres of Jupiter and Saturn: Deep atmospheric composition, cloud structure, vertical mixing, and origin, *Planet. Space Sci*., **47**, 1243–1262.

Ayliffe, B. and M. Bate (2009a), Circumplanetary disc properties obtained from radiation hydrodynamical simulations of gas accretion by protoplanets, *MNRAS*, **397**, 657–665.

(2009b), Gas accretion on to planetary cores: Three-dimensional self-gravitating radiation hydrodynamical calculations, *MNRAS*, **393**, 49–64.

(2012), The growth and hydrodynamic collapse of a protoplanet envelope, *MNRAS*, **427**, 2597–2612.

Baraffe, I., G. Chabrier and T. Barman (2008), Structure evolution of super-Earth to super-Jupiter exoplanets. I. Heavy element enrichment in the interior, *Astron. Astrophys*., **482**, 315–332.

Baraffe, I., G. Chabrier, J. Fortney et al. (2014), Planetary internal structures, in *Protostars and Planets VI*, edited by H. Beuther, R. Klessen, C. Dullemond, and Th. Henning, University of Arizona Press, Tucson, AZ.

Barstow, J. K., S. Aigrain, P. G. J. Irwin et al. (2014), Clouds on the Hot Jupiter HD189733b: Constraints from the Reflection Spectrum, *Astrophys. J*. **786**, 154.

Baruteau, C., A. Crida, S. J. Paardekooper et al. (2014), Planet-disc interactions and early evolution of planetary systems, in *Protostars and Planets VI*, edited by H. Beuter, R. Klessen, C. Dullemond, and T. Henning. University of Arizona Press, Tucson, AZ.

Bate, M. R., S. H. Lubow, G. I. Ogilvie et al. (2003), Three-dimensional calculations of high- and low-mass planets embedded in protoplanetary discs, *MNRAS*, **341**, 213–229.

Batygin, K. and D. J. Stevenson (2010), Inflating hot Jupiters with ohmic dissipation, *Astrophys. J*., **714**, L238–L243.

Birkby, J. L., R. J. de Kok, M. Brogi et al. (2013), Detection of water absorption in the day side atmosphere of HD 189733 b using ground-based high-resolution spectroscopy at 3.2 μm, *MNRAS*, **436**, 35–39.

Bitsch, B., A. Crida, A. Morbidelli et al. (2013), Stellar irradiated discs and implications on migration of embedded planets. I. Equilibrium discs, *Astron. Astrophys*., **549**, A124–137.

Bitsch, B., A. Morbidelli, E. Lega et al. (2014), Stellar irradiated discs and implications on migration of embedded planets. II. Accreting-discs, *Astron. Astrophys*., **564**, A135–146.

Black, D. C. (1972), The origins of trapped helium, neon, and argon isotopic variations in meteorites-I, *Geochim. Cosmochim. Acta*, **36**, 347–375.

Bockelée-Morvan, D., N. Biver, E. Jehin et al. (2008), Large excess of heavy nitrogen in both hydrogen cyanide and cyanogen from comet 17P/Holmes, *Astrophys. J*., **679**, L49–L52.

Bolton, S. J., S. Adriani, V. Adumitroaie, M. Allison, J. Anderson, S. K. Atreya et al. (2017), Jupiter's interior and deep atmosphere: the initial pole-to-pole passes with the Juno spacecraft, *Science*, **356**, 821–825.

Bodenheimer, P., D. N. C. Lin and R. A. Mardling (2001), On the tidal inflation of short-period extrasolar planets, *Astrophys. J*., **548**, 466–472.

Boss, A. P. (2000), Possible rapid gas giant planet formation in the solar nebula and other protoplanetary disks, *Astrophys. J*., **536**, L101–L104.

Briggs, F. H. and P. D. Sackett (1989), Radio observations of Saturn as a probe of its atmosphere and cloud structure, *Icarus*, **80**, 77–103.

Brogi, M., L. A. G. Snellen, R. J. de Kok et al. (2012), The signature of orbital motion from the dayside of the planet τ Boötis b, *Nature*, **486**, 502–504.

Burrows, A., I. Hubeny, J. Budaj et al. (2007), Possible solutions to the radius anomalies of transiting giant planets, *Astrophys. J.*, **661**, 502–514.
Cameron, A. G. W. (1973), Abundances of the elements in the solar system, *Space Sci. Rev.* **15**, 121–146.
(1979), The interaction between giant gaseous protoplanets and the primitive solar nebula, *The Moon and the Planets*, **21**, 173–183.
(1982), Elemental and nuclidic abundances in the solar system, in *Essays in Nuclear Astrophysics*, edited by W. A. Fowler, pp. 23–43, Cambridge University Press.
Canup, R. M. (2010), Origin of Saturn's rings and inner moons by mass removal from a lost Titan-sized satellite, *Nature*, **468**, 943–946.
Canup, R. M. and W. R. Ward (2002), Formation of the Galilean satellites: Conditions of accretion, *Astron. J.*, **124**, 3404–3423.
Castillo-Rogez, J., T. V. Johnson, M. H. Lee et al. (2009), ^{26}Al decay: Heat production and a revised age for Iapetus, *Icarus*, **204**, 658–662.
Charbonneau, D., H. A. Knutson, T. Barman et al. (2008), The broadband infrared emission spectrum of the exoplanet HD 189733b, *Astrophys. J.*, **686**, 2, 1341–1348.
Charnoz, S., A. Crida, J. C. Castillo-Rogez et al. (2011), Accretion of Saturn's mid-sized moons during the viscous spreading of young massive rings: Solving the paradox of silicate-poor rings versus silicate-rich moons, *Icarus*, **216**, 535–550.
Charnoz, S., J. Salmon and A. Crida (2010), The recent formation of Saturn's moonlets from viscous spreading of the main rings, *Nature*, **465**, 752–754.
Chiang, E. and P. Goldreich (1997), Spectral energy distributions of T Tauri stars with passive circumstellar disks, *Astrophys. J.*, **490**, 368–376.
Chick, K. M. and P. Cassen (1997), Thermal processing of interstellar dust grains in the primitive solar environment, *Astrophys. J.*, **477**, 398–409.
Conrath, B. J. and D. Gautier (2000), Saturn helium abundance: A reanalysis of Voyager measurements, *Icarus*, **144**, 124–134.
Conrath, B. J., D. Gautier, R. A. Hanel et al. (1984), The helium abundance of Saturn from Voyager measurements, *Astrophys. J.*, **282**, 807–815.
Conrath, B. J., R. A. Hanel and R. E. Samuelson (1989), Thermal structure and heat balance of the outer planets, in *Origin and Evolution of Planetary and Satellite Atmospheres*, edited by. S. K. Atreya, J. B. Pollack, and M. S. Matthews, pp. 513–538, University of Arizona Press, Tucson, AZ.
Cossou, C., S. Raymond and A. Pierens (2013), Convergence zones for Type I migration: An inward shift for multiple planet systems, *Astron. Astrophys.*, **553**, L2 (5 pp.).
Crida, A. and K. Batygin (2014), Spin-Orbit angle distribution and the origin of (mis)aligned hot Jupiters, *Astron. Astrophys.*, **567**, A42 (8 pp.).
Crida, A. and S. Charnoz (2012), Formation of regular satellites from ancient massive rings in the solar system, *Science*, **338**, 1196–1199.
Crida, A. and A. Morbidelli (2007), Cavity opening by a giant planet in a protoplanetary disc and effects on planetary migration, *MNRAS*, **377**, 1324–1336.
Crida, A., A. Morbidelli and F. Masset (2006), On the width and shape of gaps in protoplanetary disks, *Icarus*, **181**, 587–604.
Croll, B., D. Lafreniere, L. Albert et al. (2011), Near-infrared thermal emission from WASP-12b: Detections of the secondary eclipse in Ks, H, and J, *Astron. J.*, **141**, 30–42.
Currie, T., A. Burrows, Y. Itoh et al. (2011), A combined Subaru/VLT/MMT 1–5 μm study of planets orbiting HR 8799: Implications for atmospheric properties, masses, and formation, *Astrophys. J.*, **729**, 128–147.
Dahmen, G., T. L. Wilson and F. Matteucci (1995), The nitrogen isotope abundance in the galaxy 1: The galactic disk gradient, *Astron. Astrophys.*, **295**, 194–198.
Dartois, E., A. Dutrey and S. Guilloteau (2003), Structure of the DM Tau outer disk: probing the vertical kinetic temperature gradient, *Astron. Astrophys.*, **399**, 773–787.
Delgado-Mena, E., G. Israelian, J. I. González Hernández et al. (2010), Chemical clues on the formation of planetary systems: C/O versus Mg/Si for HARPS GTO sample, *Astrophys. J.*, **725**, 2349–2358.
Deming, D., A. Wilkins, P. McCullough et al. (2013), Infrared transmission spectroscopy of the exoplanets HD 209458b and XO-1b using the wide field camera-3 on the Hubble Space Telescope, *Astrophys. J.*, **774**, 95–112.
Demory, B. J., J. de Wit, N. Lewis et al. (2013), Inference of inhomogeneous clouds in an exoplanet atmosphere, *Astrophys. J. Lett.*, **776**, L25 (7 pp.).
de Pater, I. and S. T. Massie (1985), Models of the millimeter-centimeter spectra of the giant planets, *Icarus*, **62**, 143–171.
Dodson-Robinson, S. E., P. Bodenheimer, G. Laughlin et al. (2008), Saturn forms by core accretion in 3.4 Myr, *Astrophys. J.*, **688**, L99–L102.
Dubrulle, B., G. Morfill and M. Sterzik (1995), The dust subdisk in the protoplanetary nebula, *Icarus*, **114**, 237–246.
Dürmann, C. and W. Kley (2015), Migration of massive planets in accreting disks, *Astron. Astrophys.*, **574**, A52.
Dyudina, U. A., A. P. Ingersoll, S. P. Ewald et al. (2010), Detection of visible lightning on Saturn, *Geophys. Res. Lett.*, **37**, L09205.
(2013), Saturn's visible lightning, its radio emissions, and the structure of the 2009–2011 lightning storms, *Icarus*, **226**, 1020–1037.
Eberhardt, P. (1974), A Neon-E-rich phase in the orgueil carbonaceous chondrite, *Earth Planet. Sci. Lett.*, **24**, 182–187.
Estrada, P. R., I. Mosqueira and S. Charnoz (2009), The Ganymede, Titan, Callisto, Iapetus trend: Interpretation of Iapetus' composition, *AGU Fall Meeting Abstracts*, C1148.
Evans, T. M., F. Pont, D. K. Sing et al. (2013), The deep blue color of HD 189733b: albedo measurements with Hubble Space Telescope/space telescope imaging

spectrograph at visible wavelengths, *Astrophys. J. Lett*. **772**, L16 (5 pp.).
Fabrycky, D. and S. Tremaine (2007), Shrinking binary and planetary orbits by Kozai cycles with Tidal friction, *Astrophys. J*., **669**, 1298–1315.
Fegley, B. and R. G. Prinn (1985), Equilibrium and nonequilibrium chemistry of Saturn's atmosphere: Implications for the observability of PH_3, N_2, CO, and GeH_4, *Astrophys. J*., **299**, 1067–1078.
Flasar, F. M., R. K. Achterberg, B. J. Conrath et al. (2005), Temperatures, winds, and composition in the Saturnian system, *Science*, **307**, 1247–1251.
Fletcher, L. N., K. H. Baines, T. W. Momary et al. (2011), Saturn's tropospheric composition and clouds from Cassini/VIMS 4.6–5.1 μm nightside spectroscopy, *Icarus*, **214**, 510–533.
Fletcher, L. N., T. K. Greathouse, G. S. Orton et al. (2014), The origin of nitrogen on Jupiter and Saturn from the $^{15}N/^{14}N$ ratio, *Icarus*, **238**, 170–190.
Fletcher, L. N., G. S. Orton, N. A. Teanby et al. (2009a), Phosphine on Jupiter and Saturn from Cassini/CIRS, *Icarus*, **202**, 543–564.
(2009b), Methane and its isotopologues on Saturn from Cassini/CIRS Observations, *Icarus*, **199**, 351–367.
Folkner, W. M., R. Woo and S. Nandi (1998), Ammonia abundance in Jupiter's atmosphere derived from attenuation of the Galileo Probe's radio signal, *J. Geophys. Res*., **103**, 22847–22856.
Fortney, J. J., K. Lodders, M. S. Marley et al. (2008), A unified theory for the atmospheres of the hot and very hot Jupiters: Two classes of irradiated atmospheres, *Astrophys. J*., **678**, 1419–1435.
Fouchet, T., E. Lellouch, B. Bezard et al. (2000), ISO-SWS observations of Jupiter: measurement of the ammonia tropospheric profile and of the $^{15}N/^{14}N$ isotopic ratio, *Icarus*, **143**, 223–243.
Fujii, Y. I., S. Okuzumi and S. Inutsuka (2011), A fast and accurate calculation scheme for ionization degrees in protoplanetary and circumplanetary disks with charged dust grains, *Astrophys. J*., **743**, 53–61.
Fujii, Y. I., S. Okuzumi, T. Tanigawa et al. (2014), On the viability of the magnetorotational instability in circumplanetary disks, *Astrophys. J*., **785**, 101–108.
Gaudi, B. S. and J. N. Winn (2007), Prospects for the characterization and confirmation of transiting exoplanets via the Rossiter–McLaughlin effect, *Astrophys. J*., **655**, 550–563.
Gaulme, P., F. X. Schmider, J. Gay et al. (2011), Detection of Jovian seismic waves: A new probe of its interior structure, *Astron. Astrophys*., **531**, A104 (7 pp.).
Gautier, D., F. Hersant, O. Mousis et al. (2001), Enrichments in volatiles in Jupiter: A new interpretation of the Galileo measurements. *Astrophys. J*., **550**, L227–L230.
Geiss, J. (1993), Primordial abundance of hydrogen and helium isotopes, in *Origin and Evolution of the Elements*, edited by N. Prantzos, E. Vangioni-Flam, and M. Cassé, pp. 89–106, Cambridge University Press, Cambridge.
Geiss, J. and G. Gloeckler (1998), Abundances of deuterium and helium-3 in the protosolar cloud, *Space Sci. Rev*., **84**, 239–250.
Geiss, J. and H. Reeves (1972), Cosmic and solar system abundances of deuterium and helium-3, *Astron. Astrophys*., **18**, 126–132.
Gibb, E. L., D. C. B. Whittet, A. C. A. Boogert et al. (2004), Interstellar ice: The infrared space observatory legacy, *Astrophys. J. Supp. Ser*., **151**, 35–73.
Gorti, U., C. P. Dullemond and D. Hollenbach (2009), Time evolution of viscous circumstellar disks due to photoevaporation by far-ultraviolet, extreme-ultraviolet, and X-ray radiation from the central star, *Astrophys. J*., **705**, 1237–1251.
Grevesse, N., M. Asplund and A. J. Sauval (2005), The new solar chemical composition, in Elements Stratification in Stars, 40 Years of Atomic Diffusion, edited by G. Alecian, O. Richard, and S. Vauclair, **17**, pp. 21–30, *EAS Publications Series*.
(2007), The solar chemical composition, *Space Sci. Rev*., **130**, 105–114.
Grossman, A. S., J. B. Pollack, R. T. Reynolds et al. (1980), The effect of dense cores on the structure and evolution of Jupiter and Saturn, *Icarus*, **42**, 358–379.
Guillot, T. and R. Hueso (2006), The composition of Jupiter: Sign of a (relatively) late formation in a chemically evolved protosolar disc, *MNRAS*, **367**, L47–L51.
Guillot, T., N. C. Santos, F. Pont et al. (2006), A correlation between the heavy element content of transiting extrasolar planets and the metallicity of their parent stars, *Astron. Astrophys*, **453**, L21–L24.
Guillot, T. and A. P. Showman (2002), Evolution of "51 Pegasus b-like" planets, *Astron. Astrophys*., **385**, 156–165.
Guillot, T., D. J. Stevenson, W. B. Hubbard et al. (2004), The interior of Jupiter, in *Jupiter. The Planet, Satellites and Magnetosphere*, edited by F. Bagenal, T. E. Dowling, and W. B. McKinnon, pp. 35–57, Cambridge University Press, Cambridge.
Hartogh, P., D. C. Lis, D. Bockelée-Morvan et al. (2011), Ocean-like water in the Jupiter-family comet 103P/Hartley 2, *Nature*, **478**, 218–220. doi:10.1038/nature10519; pmid: 21976024.
Hayashi, C. (1981), Structure of the solar nebula, growth and decay of magnetic fields and effects of magnetic and turbulent viscosities on the nebula, *Prog. Theor. Phys. Supp*., **70**, 35–53.
Haynes, K., A. M. Mandell, N. Madhusudhan et al. (2015), Spectroscopic evidence for a temperature inversion in the dayside atmosphere of hot Jupiter WASP-33b, *Astrophys. J*., **806**, 146, 12 pp.
Helled, R. and T. Guillot (2013), Interior models of Saturn: Including the uncertainties in shape and rotation, *Astrophys. J*., **767**, 113–119.
Helled, R. and J. I. Lunine (2014), Measuring Jupiter's water abundance by Juno: The link between interior and formation models, *MNRAS*, **441**, 2273–2279.

Helling, C., P. Woitke, P. B. Rimmer et al. (2014), Disk evolution, element abundances and cloud properties of young gas giant planets, *Life*, **4**, 142–173.

Hersant, F., D. Gautier, G. Tobie et al. (2008), Interpretation of the carbon abundance in Saturn measured by Cassini, *Planet. Space Sci*., **56**, 1103–1111.

Hoffman, J. H., R. R. Hodges, M. B. McElroy et al. (1979), Composition and structure of the Venus atmosphere: Results from Pioneer Venus, *Science*, **205**, 49–52.

Howard, A. W. (2013), Observed properties of extrasolar planets, *Science*, **340**, 572–576.

Hubeny, I., A. Burrows and D. Sudarsky (2003), A possible bifurcation in atmospheres of strongly irradiated stars and planets, *Astrophys. J*., **594**, 1011–1018.

Ida, S., D. N. C. Lin and M. Nagasawa (2013), Toward a deterministic model of planetary formation. VII. Eccentricity distribution of gas giants, *Astrophys. J*., **775**, 42–66.

Ikoma, M., H. Emori and K. Nakazawa (2001), Formation of giant planets in dense nebulae: Critical core mass revisited, *Astrophys. J*., **553**, 99–1005.

Ishimaru, R., Y. Sekine, T. Matsui et al. (2011), Oxidizing proto-atmosphere on Titan: Constraint from N_2 formation by impact shock, *Astrophys. J. Lett*., **741**, L10 (6 pp.).

Janson, M., T. D. Brandt, M. Kuzuhara et al. (2013), Direct imaging detection of methane in the atmosphere of GJ 504 b, *Astrophys. J. Lett*., **778**, L4 (6 pp.).

Jewitt, D., H. E. Matthews, T. Owen et al. (1997), The $^{12}C/^{13}C$, $^{14}N/^{15}N$ and $^{32}S/^{34}S$ isotope ratios in comet Hale–Bopp (C/1995 O1), *Science*, **278**, 90–93.

Johansen, A., J. S. Oishi, M. Mac Low et al. (2007), Rapid planetesimal formation in turbulent circumstellar disks, *Nature*, **448**, 1022–1025.

Johansen, A. and A. Youdin (2007), Protoplanetary disk turbulence driven by the streaming instability: Nonlinear saturation and particle concentration, *Astrophys. J*., **662**, 627–641.

Johansen, A., A. Youdin and M. M. Mac Low (2009), Particle clumping and planetesimal formation depend strongly on metallicity, *Astrophys. J*., **704**, L75–L79.

Johnson, J. A., K. M. Aller, A. W. Howard et al. (2010), Giant planet occurrence in the stellar mass-metallicity plane, *PASP*, **122**, 905–915.

Jones, T. D. and J. S. Lewis (1987), Estimated impact shock production of N_2 and organic compounds on early Titan, *Icarus*, **72**, 381–393.

Karkoschka, E. and M. G. Tomasko (2011), The haze and methane distributions on Neptune from HST-STIS spectroscopy, *Icarus*, **211**, 328–340.

Knutson, H. A., A. W. Howard and H. Isaacson (2010), A correlation between stellar activity and hot Jupiter emission spectra, *Astrophys. J*., **720**, 1569–1576.

Kokubo, E. and S. Ida (1998), Oligarchic growth of protoplanets, *Icarus*, **131**, 171–178.

Konopacky, Q. M., T. S. Barman, B. A. Macintosh et al. (2013), Detection of carbon monoxide and water absorption lines in an exoplanet atmosphere, *Science*, **339**, 1398–1401.

Kouchi, A., T. Yamamoto, T. Kozasa et al. (1994), Conditions for condensation and preservation of amorphous ice and crystallinity of astrophysical ices, *Astron. Astrophys*., **290**, 1009–1018.

Kreidberg, L., J. L. Bean, J. M. Désert et al. (2014), A precise water abundance measurement for the hot Jupiter WASP-43b, *Astrophys J. Lett*., **793**, L27 (6 pp.).

Lainey, V., R. A. Jacobson, R. Tajeddine et al. (2015), New constraints on Saturn's interior from Cassini astrometric data. Submitted.

Lainey, V., Ö. Karatakin, J. Desmars et al. (2012), Strong tidal dissipation in Saturn and constraints on Enceladus' thermal state from astrometry, *Astrophys. J*., **752**, 14–32.

Lambrechts, M. and A. Johansen (2012), Rapid growth of gas-giant cores by pebble accretion, *Astron. Astrophys*., **544**, A32.

Lambrechts, M., A. Johansen and A. Morbidelli (2014), Separating gas-giant and ice-giant planets by halting pebble accretion, *Astron. Astrophys*., **572**, A35.

Laraia, A. L., A. P. Ingersoll, M. A. Janssen et al. (2013), Analysis of Saturn's thermal emission at 2.2-cm wavelength: Spatial distribution of ammonia vapor, *Icarus*, **226**, 641–654.

Leconte, J., G. Chabrier, I. Baraffe et al. (2010), Is tidal heating sufficient to explain bloated exoplanets? Consistent calculations accounting for finite initial eccentricity, *Astron. Astrophys*., **516**, A64 (13 pp.).

Lee, J. M., L. N. Fletcher and P. G. J. Irwin (2012), Optimal estimation retrievals of the atmospheric structure and composition of HD 189733b from secondary eclipse spectroscopy, *MNRAS*, **420**, 170–182.

Lellouch, E., B. Bézard, T. Fouchet et al. (2001), The deuterium abundance in Jupiter and Saturn from ISO-SWS observations, *Astron. Astrophys*., **370**, 610–622.

Li, C. and A. P. Ingersoll (2015), Moist convection in hydrogen atmospheres and the frequency of Saturn's giant storms, *Nat. Geosci*. **8**, 398–403.

Lin, D. N. C., P. Bodenheimer and D. C. Richardson (1996), Orbital migration of the planetary companion of 51 Pegasi to its present location, *Nature*, **380**, 606–607.

Lin, D. N. C. and J. Papaloizou (1986), On the tidal interaction between protoplanets and the protoplanetary disk. III. Orbital migration of protoplanets, *Astrophys. J*., **309**, 846–857.

Lodders, K. (2004), Jupiter formed with more tar than ice, *Astrophys. J*., **611**, 587–597.

(2008), The solar argon abundance, *Astrophys. J*., **674**, 607–611.

Lodders, K. and B. Fegley (2002), Atmospheric chemistry in giant planets, brown dwarfs, and low-mass dwarf stars. I. Carbon, nitrogen, and oxygen, *Icarus*, **155**, 393–424.

Lodders, K., H. Palme and H. P. Gail (2009), Abundances of the elements in the solar system, in *Landolt-Börnstein New Series, Astron. and Astrophys*., edited by J. E. Trümper, vol. VI/4B, pp. 560–630, Springer-Verlag, Berlin.

Lunine, J. I., S. K. Atreya and J. B. Pollack (1989), Present state and chemical evolution of the atmospheres of

Titan, Triton, and Pluto, in *Origin and Evolution of Planetary and Satellite Atmospheres*, edited by S. K. Atreya, J. B. Pollack, and M. S. Matthews, pp. 605–665, University of Arizona Press, Tucson, AZ.

Lyra, W., S. Paardekooper and M. Mac Low (2010), Orbital migration of low-mass planets in evolutionary radiative models: Avoiding catastrophic infall, *Astrophys. J. Lett*., **715**, L68–L73.

Machida, M. N., E. Kokubo, S. I. Inutsuka et al. (2008), Angular momentum accretion onto a gas giant planet, *Astrophys. J*., **685**, 1220–1236.

Macintosh, B., J. R. Graham, T. Barman et al. (2015), Discovery and spectroscopy of the young Jovian planet 51 Eri b with the Gemini Planet Imager, *Science*, **350**, 64–67.

Madhusudhan, N. (2012), C/O ratio as a dimension for characterizing exoplanetary atmospheres, *Astrophys. J*., **758**, 36–57.

Madhusudhan, N., M. A. Amin and G. M. Kennedy (2014c), Toward chemical constraints on hot Jupiter migration, *Astrophys. J. Lett*., **794**, 12.

Madhusudhan, N., N. Crouzet, P. R. McCullough et al. (2014a), H_2O abundances in the atmospheres of three hot Jupiters, *Astrophys. J. Lett*., **791**, L9 (5 pp.).

Madhusudhan, N., J. Harrington, K. B. Stevenson et al. (2011a), A high C/O ratio and weak thermal inversion in the atmosphere of exoplanet WASP-12b, *Nature*, **469**, 64–67.

Madhusudhan, N., H. Knutson, J. Fortney et al. (2014b), Exoplanetary atmospheres, in *Protostars and Planets VI*, edited by H. Beuther, R. Klessen, C. Dullemond, and Th. Henning, University of Arizona Press, Tucson, AZ.

Madhusudhan, N., O. Mousis, T. V. Johnson et al. (2011b), Carbon-rich giant planets: atmospheric chemistry, thermal inversions, spectra, and formation conditions, *Astrophys. J*., **743**, 191–202.

Madhusudhan N. and S. Seager (2010), On the inference of thermal inversions in hot Jupiter atmospheres, *Astrophys. J*., **725**, 261–274.

Mahaffy, P. R., T. M. Donahue, S. K. Atreya et al. (1998), Galileo Probe measurements of D/H and ^{3}He/^{4}He in Jupiter's atmosphere, *Space Sci. Rev.*, **84**, 251–263.

Mahaffy, P. R., H. B. Niemann, A. Alpert et al. (2000), Noble gas abundances and isotope ratios in the atmosphere of Jupiter from the Galileo probe mass spectrometer, *J. Geophys. Res*. (*Planets*), **105 (E6)**, 15061–15071.

Mahaffy, P. R., C. R. Webster, J. C. Stern et al. (2014), The imprint of atmospheric evolution in the D/H of Hesperian clay minerals on Mars, *Science*, **347**, 415–417.

Mandell, A., K. Haynes, E. Sinukoff et al. (2013), Exoplanet transit spectroscopy using WFC3: WASP-12 b, WASP-17 b, and WASP-19 b, *Astrophys. J*., **779**, 128.

Mandt, K. E., O. Mousis, J. I. Lunine et al. (2014), Protosolar ammonia as the unique source of Titan's nitrogen, *Astrophys. J. Lett*., **788**, L24 (5 pp.).

Marboeuf, U., A. Thiabaud, A. Alibert et al. (2014), From stellar nebula to planetesimals, *Astron. Astrophys*., **570**, 35.

Marley, M. S., D. Saumon, M. Cushing et al. (2012), Masses, radii, and cloud properties of the HR 8799 planets, *Astrophys. J*., **753**, 135–152.

Marois, C., B. Zuckerman, Q. M. Konopacky et al. (2010), Images of a fourth planet orbiting HR 8799, *Science*, **468**, 1080–1083.

Marty, B., M. Chaussidon, R. C. Wiens et al. (2011), A ^{15}N-poor isotopic composition for the solar system as shown by genesis solar wind samples, *Science*, **332**, 1533–1536.

Masset, F. and M. Snellgrove (2001), Reversing type II migration: Resonance trapping of a lighter giant protoplanet, *MNRAS*, **320**, L55–L59.

Mathew, K. J. and K. Marti (2001), Early evolution of Martian volatiles: Nitrogen and noble gas components in ALH84001 and Chassigny, *J. Geophys. Res*., **106**, 1401–1422.

Matter, A., T. Guillot and A. Morbidelli (2009), Calculation of the enrichment of the giant planet envelopes during the "late heavy bombardment," *Planet. Space Sci*., **57**, 816–821.

Mayer, L., T. Quinn, K. Wadsley et al. (2002), Formation of giant planets by fragmentation of protoplanetary disks, *Science*, **298**, 1756–1759.

McCullough, P. R., N. Crouzet, D. Deming et al. (2014), Water vapor in the spectrum of the extrasolar planet HD 189733b: 1. The transit, *Astrophys. J*., **791**, 55.

McKay, C. P., T. W. Scattergood, J. B. Pollack et al. (1988), High-temperature shock formation of N_2 and organics on primordial Titan, *Nature*, **332**, 520–522.

Menou, K. (2012), Thermo-resistive instability of hot planetary atmospheres, *Astrophys. J*., **754**, L9–L14.

Mizuno, H. (1980), Formation of the giant planets, *Progr. Theor. Phys*. **64**, 544–557.

Morbidelli, A. and A. Crida (2007), The dynamics of Jupiter and Saturn in the gaseous protoplanetary disk, *Icarus*, **191**, 158–171.

Morbidelli, A. and D. Nesvorny (2012), Dynamics of pebbles in the vicinity of a growing planetary embryo: Hydro-dynamical simulations, *Astron. Astrophys*., **546**, A18–25.

Morbidelli, A., J. Szulágyi, A. Crida et al. (2014), Meridional circulation of gas into gaps opened by giant planets in three-dimensional low-viscosity disks, *Icarus*, **232**, 266–270.

Mordasini, C., Y. Alibert and W. Benz (2009), Extrasolar planet population synthesis. I. Method, formation, tracks, and mass-distance distribution, *Astron. Astrophys*., **501**, 1139–1160.

Moses, J. I., N. Madhusudhan, C. Visscher et al. (2013), Chemical consequences of the C/O ratio on hot Jupiters: Examples from WASP-12b, CoRoT-2b, XO-1b, and HD 189733b, *Astrophys. J*., **763**, 25–51.

Mousis, O., Y. Alibert and W. Benz (2006), Saturn's internal structure and carbon enrichment, *Astron. Astrophys*., **449**, 411–415.

Mousis, O., D. Gautier and D. Bockelée-Morvan (2002), An evolutionary turbulent model of Saturn's subnebula:

Implications for the origin of the atmosphere of Titan, *Icarus*, **156**, 162–175.
Mousis, O., J. I. Lunine, N. Madhusudhan et al. (2012), Nebular water depletion as the cause of Jupiter's low oxygen abundance, *Astrophys. J.* **751**, L7 (5 pp.).
Mousis, O., J. I. Lunine, M. Pasek et al. (2009a), A primordial origin for the atmospheric methane of Saturn's moon Titan, *Icarus*, **204**, 749–751.
Mousis, O., J. I. Lunine, C. Thomas et al. (2009b), Clathration of volatiles in the solar nebula and implications for the origin of Titan's atmosphere, *Astrophys. J.*, **691**, 1780–1786.
Mousis, O., U. Marboeuf, J. I. Lunine et al. (2009c), Determination of the minimum masses of heavy elements in the envelopes of Jupiter and Saturn, *Astrophys. J.*, **696**, 1348–1354.
Nettelmann, N., R. Püstow and R. Redmer (2013), Saturn layered structure and homogeneous evolution models with different EOSs, *Icarus*, **225**, 548–557.
Niemann, H. B., S. K. Atreya, S. J. Bauer et al. (2005), The abundances of constituents of Titan's atmosphere from the GCMS instrument on the Huygens probe, *Nature*, **438**, 779–784.
Niemann, H. B., S. K. Atreya, G. R. Carignan et al. (1998), The composition of the jovian atmosphere as determined by the Galileo probe mass spectrometer, *J. Geophys. Res.*, **103**, 22831–22845.
Niemann, H. B., S. K. Atreya, J. E. Demick et al. (2010), The composition of Titan's lower atmosphere and simple surface volatiles as measured by the Cassini–Huygens probe gas chromatograph mass spectrometer experiment, *J. Geophys. Res. (Planets)*, **115**, E12006.
Notesco, G. and A. Bar-Nun (2005), A ~25 K temperature of formation for the submicron ice grains which formed comets, *Icarus*, **175**, 546–550.
Öberg, K. I., A. C. A. Boogert, K. M. Pontoppidan et al. (2011a), II, The Spitzer ice legacy: Ice evolution from cores to protostars, *Astrophys. J.*, **740**, 109–124.
Öberg, K. I., R. Murray-Clay and E. A. Bergin (2011b), The effects of snowlines on C/O in planetary atmospheres, *Astrophys. J. Lett.*, **743**, L16 (5 pp.).
Owen, T. and T. Encrenaz (2006), Compositional constraints on the giant planet formation, *Planet. Space Sci.* **54**, 1188–1196.
Owen, T., P. Mahaffy, H. Niemann et al. (1999), A low-temperature origin for the planetesimals that formed Jupiter, *Nature*, **402**, 269–270.
(2001), Protosolar nitrogen, *Astophys. J.*, **553**, L77–L79.
Paardekooper, S. J., C. Baruteau, A. Crida et al. (2010), A torque formula for non-isothermal type I planetary migration: I. Unsaturated horseshoe drag, *MNRAS*, **401**, 1950–1964.
Paardekooper, S. J., C. Baruteau and W. Kley (2011), A torque formula for non-isothermal Type I planetary migration: II. Effects of diffusion, *MNRAS*, **410**, 293–303.
Paardekooper, S. J. and G. Mellama (2006), Halting type I planet migration in non-isothermal disks, *Astron. Astrophys.*, **459**, L17–L20.
Palme, H. and A. Jones (2003), Solar system abundances of the elements, in *Treatise on Geochemistry*, edited by H. D. Holland and K. Turekian, Elsevier, pp. 41–61.
Papaloizou, J. and D. N. C. Lin (1984), On the tidal interaction between protoplanets and the primordial solar nebula: I. Linear calculation of the role of angular momentum exchange, *Astrophys. J.*, **285**, 818–834.
Pollack, J. B., O. Hubickyj, P. Bodenheimer et al. (1996), Formation of the giant planets by concurrent accretion of solids and gas, *Icarus*, **124**, 62–85.
Pont, F., D. K. Sing, N. P. Gibson et al. (2013), The prevalence of dust on the exoplanet HD 189733b from Hubble and Spitzer observations, *Mon. Not. R. Astron. Soc.*, **432**, 2917–2944.
Prinn, R. G. and B. Fegley (1981), Kinetic inhibition of CO and N_2 reduction in circumplanetary nebulae: Implications for satellite composition, *Astrophys. J.*, **249**, 308–317.
(1989), Solar nebula chemistry: Origins of planetary, satellite and cometary volatiles, in *Origin and Evolution of Planetary and Satellite Atmospheres*, edited by S. K. Atreya, J. B. Pollack, and M. S. Matthews, pp. 78–136, University of Arizona Press, Tucson, AZ.
Rasio, F. A. and E. B. Ford (1996), Dynamical instabilities and the formation of extrasolar planetary systems, *Science*, **274**, 954–956.
Redfield, S., M. Endl, W. D. Cochran et al. (2008), Sodium absorption from the exoplanetary atmosphere of HD 189733b detected in the optical transmission spectrum, *Astrophys. J.*, **673**, L87–L90.
Remus, F., S. Mathis, J. P. Zahn et al. (2012), Anelastic tidal dissipation in multi-layer planets, *Astron. Astrophys.*, **541**, A165 (17 pp.).
Rivier, G., A. Crida, A. Morbidelli et al. (2012), Circumplanetary discs as bottlenecks for gas accretion onto giant planets, *Astron. Astrophys.*, **548**, A116 (7 pp.).
Rosman, K. J. R. and P. D. P. Taylor (1998), Isotopic compositions of the elements, *J. Phys. Chem. Ref. Data*, **27**, 1275–1287.
Roulston, M. S. and D. J. Stevenson (1995), Prediction of neon depletion in Jupiter's atmosphere (abstract), *EOS Abstr., AGU Fall Mtg.*, **76**, 343.
Rousselot, P., O. Pirali, E. Jehin et al. (2014), Toward a unique nitrogen isotopic ratio in cometary ices, *Astrophys. J. Lett*, **780**, L17 (5 pp.).
Salmon, J., S. Charnoz, A. Crida et al. (2010), Long-term and large-scale viscous evolution of dense planetary rings, *Icarus*, **209**, 771–785.
Seager, S. and D. Sasselov (2000), Theoretical transmission spectra during extrasolar giant planet transits, *Astrophys. J.*, **537**, 916–921.
Sekine, Y., H. Genda, S. Sugita et al. (2011), Replacement and late formation of atmospheric N_2 on undifferentiated Titan by impacts, *Nature Geoscience*, **4**, 359–362.
Sekine, Y., S. Sugita, T. Shido et al. (2005), The role of Fischer Tropsch catalysis in the origin of methane-rich Titan, *Icarus*, **178**, 154–164.
Sing, D. K., F. Pont, S. Aigrain et al. (2011), Hubble Space Telescope transmission spectroscopy of the exoplanet

HD 189733b: High-altitude atmospheric haze in the optical and near-ultraviolet with STIS, *Mon. Not. R. Astron. Soc*., **416**, 1443–1455.

Snellen, I. A. G., R. J. de Kok, E. J. W. de Mooij et al. (2010), The orbital motion, absolute mass and high-altitude winds of exoplanet HD209458b, *Nature*, **465**, 1049–1053.

Spiegel, D. S. and A. Burrows (2013), Thermal processes governing hot-Jupiter radii, *Astrophys. J*., **772**, 76–89.

Spiegel, D. S., K. Silverio and A. Burrows (2009), Can TiO explain thermal inversions in the upper atmospheres of irradiated giant planets?, *Astrophys. J*., **699**, 1487–1500.

Sromovsky, L. A., P. M. Fry and J. H. Kim (2011), Methane on Uranus: The case for a compact CH_4 cloud layer at low latitudes and a severe CH_4 depletion at high-latitudes based on re-analysis of Voyager occultation measurements and STIS spectroscopy, *Icarus*, **215**, 292–312.

Stevenson, K. B., J.-M. Desert, M. R. Line et al. (2014), Thermal structure of an exoplanet atmosphere from phase-resolved emission spectroscopy, *Science*, **346**, 838–841.

Sudarsky, D., A. Burrows and I. Hubeny (2003), Theoretical spectra and atmospheres of extrasolar giant planets, *Astrophys. J*., **588**, 1121–1148.

Sumi, T., K. Kamiya, A. Udalski et al. (2011), Unbound or distant planetary mass population detected by gravitational microlensing, *Nature*, **473**, 349–352.

Szula×i, J., A. Morbidelli, A. Crida et al. (2014), Accretion of Jupiter-mass planets in the limit of vanishing viscosity, *Astrophys. J*., **782**, 65–75.

Tanigawa, T., K. Ohtsuki and M. N. Machida (2012), Distribution of accreting gas and angular momentum onto circumplanetary disks, *Astrophys. J*., **747**, 47–62.

Triaud, A. H. M. J., A. Collier Cameron, D. Queloz et al. (2010), Spin-orbit angle measurements for six southern transiting planets: New insights into the dynamical origins of hot Jupiters, *Astron. and Astrophys*, **524**, A25.

Tsiganis, K., R. Gomes, A. Morbidelli et al. (2005), Origin of the orbital architecture of the giant planets of the Solar System, *Nature*, **435**, 459–461.

Turner N. J., S. Fromang, C. Gammie et al. (2014), Transport and accretion in planet-forming disks, in *Protostars and Planets VI*, edited by H. Beuter, R. Klessen, C. Dullemond, and T. Henning. University of Arizona Press, Tucson, AZ.

Turner, N. J., M. H. Lee and T. Sano (2010), The formation environment of the Galilean moons. American Astronomical Society, DPS Meeting No. 42, Abst. 24.08.

(2014), Magnetic coupling in the disks around young gas giant planets, *Astrophys. J*., **783**, 14–28.

Vidal-Madjar, A., A. Lecavelier des Etangs, J. M. Désert et al. (2003), An extended upper atmosphere around the extrasolar planet HD209458b, *Nature*, **422**, 143–146.

Visscher, C. and B. Fegley (2005), Chemical constraints on the water and total oxygen abundances in the deep atmosphere of Saturn, *Astrophys. J*., **623**, 1221–1227.

Vogel, N., V. S. Heber, H. Baur et al. (2011), Argon, krypton, and xenon in the bulk solar wind as collected by the genesis mission, *Geochim. Cosmochim. Acta*, **75**, 3057–3071.

von Zahn, U., D. M. Hunten and G. Lehmacher (1998), Helium in Jupiter's atmosphere: results from the Galileo probe helium interferometer experiment, *J. Geophys. Res*., **103**, 22815–22830.

von Zahn, U., S. Komer, H. Wieman et al. (1983), Composition of the Venus atmosphere, in *Venus*, edited by D. M. Hunten, L. Colin, T. M. Donahue, and V. I. Moroz, pp. 297–430, University of Arizona Press, Tucson, AZ.

Walsh, K., A. Morbidelli, S. N. Raymond et al. (2011), A low mass for Mars from Jupiter's early gas-driven migration, *Nature*, **475**, 206–209.

Ward, W. R. (1997), Protoplanet migration by nebula tides, *Icarus*, **126**, 261–281.

Webster, C. R., P. R. Mahaffy, G. J. Flesch et al. (2013), Isotope ratios of H, C, and O in CO_2 and H_2O of the martian atmosphere, *Science*, **341**, 260–263.

Weidenschilling, S. J. (1984), Evolution of grains in a turbulent solar nebula, *Icarus*, **60**, 553–568.

Wilson, H. F. and B. Militzer (2010), Sequestration of noble gases in giant planet interiors, *Phys. Rev. Lett*., **104**, 121101 (4 pp.).

(2012), Solubility of water ice in metallic hydrogen: Consequences for core erosion in gas giant planets, *Astrophys. J*., **745**, 54–58.

Winn, J. N., D. Fabrycky, S. Albrecht et al. (2010), Hot stars with hot Jupiters have high obliquities, *Astrophys. J. Lett*., **718**, L145–L149.

Wong, M. H., S. K. Atreya, W. R. Kuhn et al. (2015), Fresh clouds: A parameterized updraft method for calculating cloud densities in one-dimensional models, *Icarus*, **245**, 273–281.

Wong, M. H., S. K. Atreya, P. N. Mahaffy et al. (2013), Isotopes of nitrogen on Mars: atmospheric measurements by Curiosity's mass spectrometer, *Geophys. Res. Lett*., **40**, 6033–6037.

Wong, M. H., P. R. Mahaffy, S. K. Atreya et al. (2004), Updated Galileo probe mass spectrometer measurements of carbon, oxygen, nitrogen, and sulfur on Jupiter, *Icarus*, **171**, 153–170.

Youdin, A. N. and J. Goodman (2005), Streaming instabilities in protoplanetary disks, *Astrophys. J*., **620**, 459–469.

Youdin, A. N. and J. L. Mitchell (2010), The mechanical greenhouse: Burial of heat by turbulence in hot Jupiter atmospheres, *Astrophys. J*., **721**, 1113–1126.

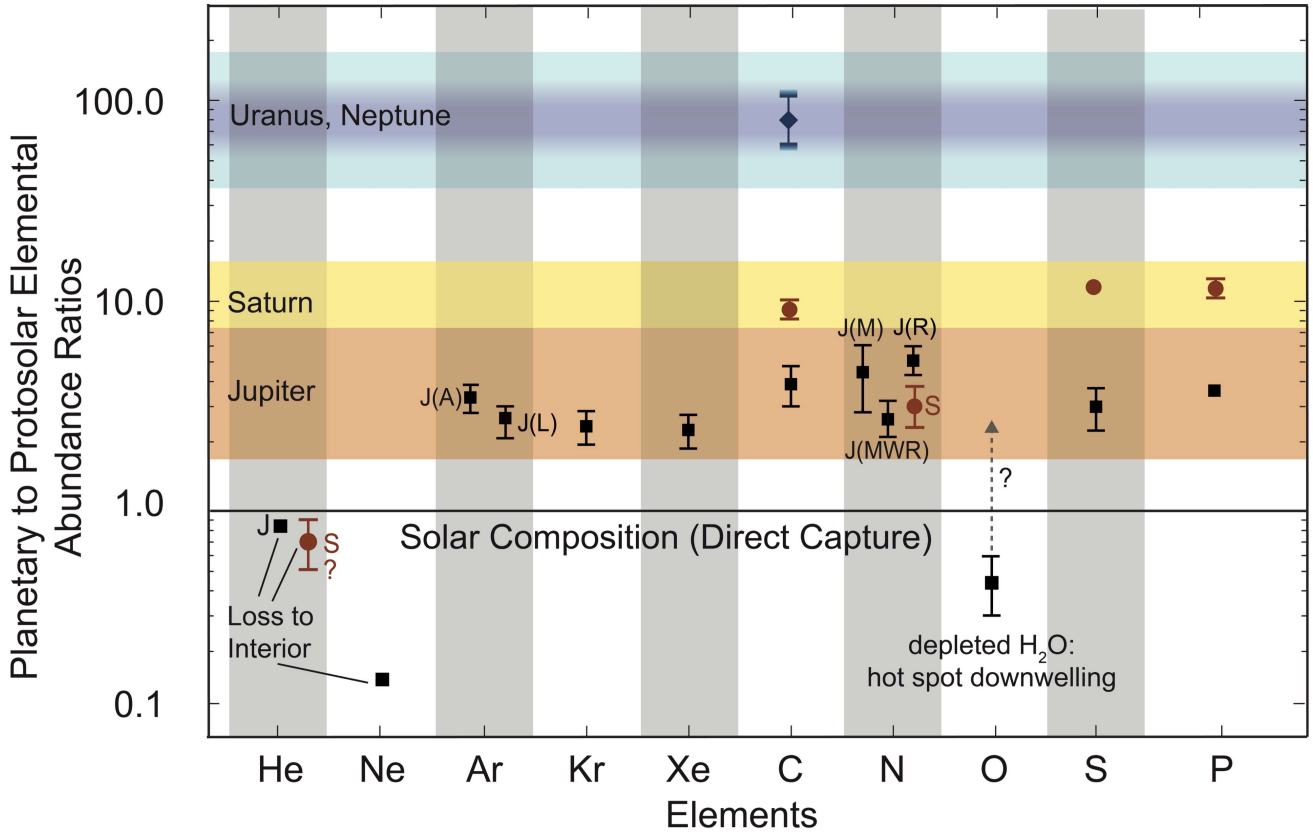

Figure 2.1

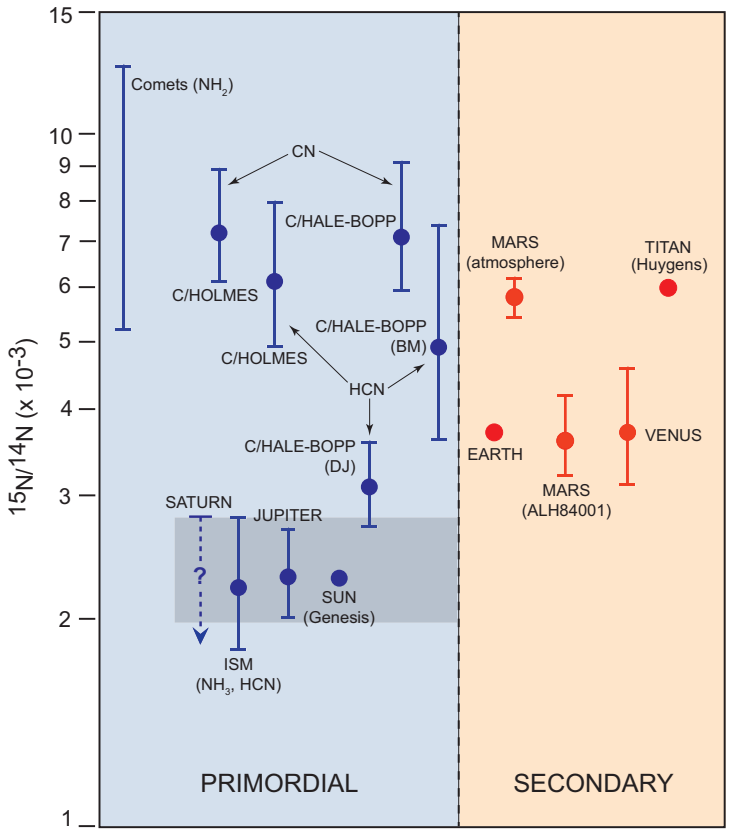

Figure 2.3

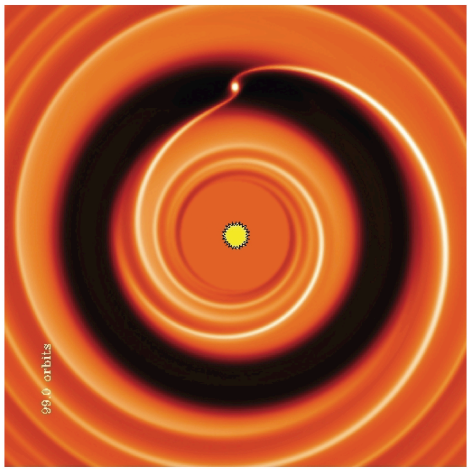

Figure 2.4

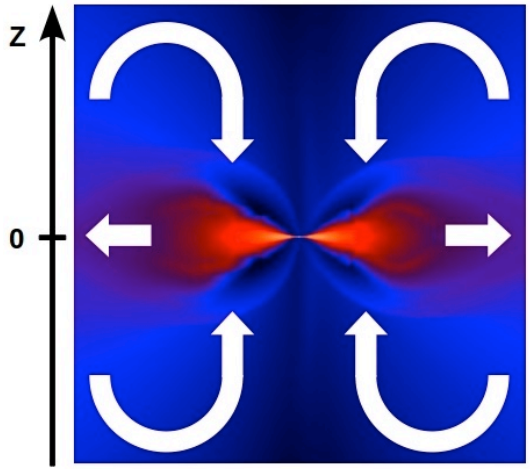

Figure 2.5

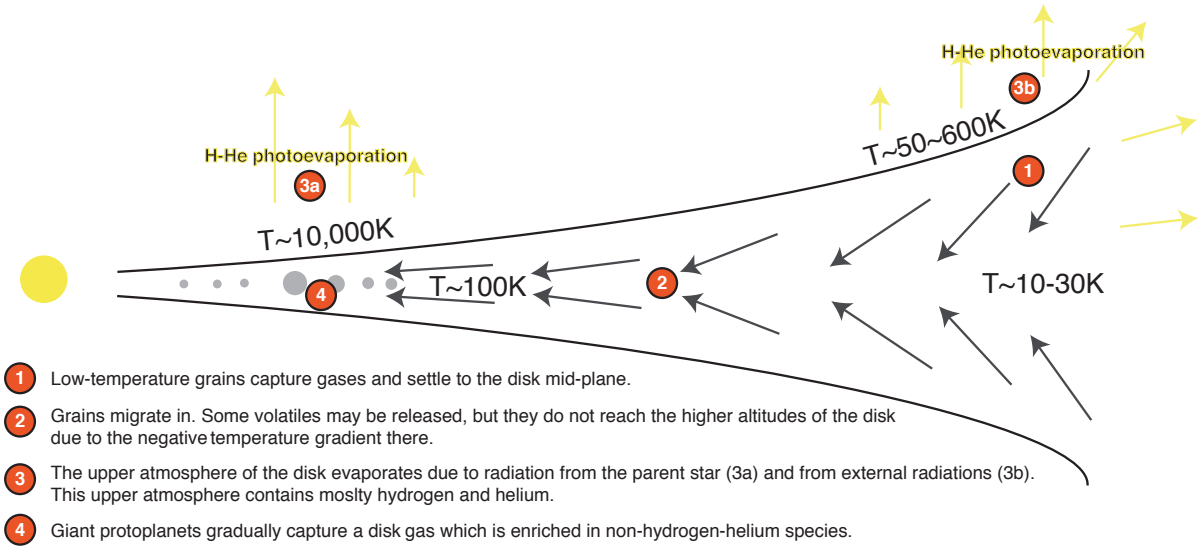

1. Low-temperature grains capture gases and settle to the disk mid-plane.
2. Grains migrate in. Some volatiles may be released, but they do not reach the higher altitudes of the disk due to the negative temperature gradient there.
3. The upper atmosphere of the disk evaporates due to radiation from the parent star (3a) and from external radiations (3b). This upper atmosphere contains moslty hydrogen and helium.
4. Giant protoplanets gradually capture a disk gas which is enriched in non-hydrogen-helium species.

Figure 2.8

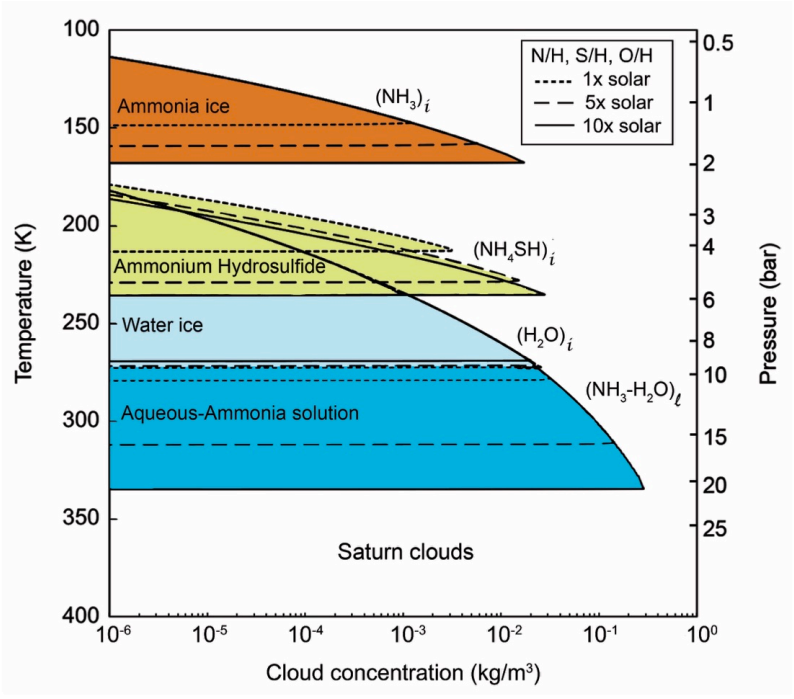

Figure 2.9